JET BREAKUP AND PINCH-OFF IN

LIQUID-LIQUID SYSTEMS

TODD EDWIN CRANE

B.S. AEROSPACE ENGINEERING
OKLAHOMA STATE UNIVERSITY
2002

B.S. MECHANICAL ENGINEERING
OKLAHOMA STATE UNIVERSITY
2002

This work is submitted to the Faculty of the Graduate
College of Oklahoma State University in partial
fulfillment of the requirements for the degree
of MASTER OF SCIENCE
July 2006

JET BREAKUP AND PINCH-OFF IN

LIQUID-LIQUID SYSTEMS

Thesis Approved:

Dr. Khaled A. Sallam, Thesis Advisor

Dr. Afshin J. Ghajar, Committee Member

Dr. Frank W. Chambers, Committee Member

A. Gordon Emslie, Dean of the Graduate College

Acknowledgments

The author would like to acknowledge his advisor, Dr. Khaled A. Sallam, for his advice and encouragement during the period of this research at Oklahoma State University. The author is also grateful for Dr. Afshin J. Ghajar and Dr. Frank W. Chambers for their participation on this thesis committee.

The author would especially like to thank his wife, Allison, and son, Parker, for their support and understanding of the demands that had to be met in order to make this project successful. He would also like to acknowledge his daughter, Brooklynn, and thank her for her impeccable timing in deciding when to come into this world.

Table of Contents

Table of Figures

List of Tables

Nomenclature

Alphabetical

Bo	Bond Number	$= \frac{\Delta\rho D^2}{\sigma}$
Capillary	thin thread joining the main jet to the separating droplet	
Ca	Capillary number	$= \frac{\mu U_e}{\sigma}$
Cone Angle	total enclosed angle formed by a pinch-off event, also called pinch-off angle	
d_e	nozzle exit diameter = D	
d_d	equilibrium drop diameter of primary (parent) droplet	
d_d^*	drop diameter measured in last frame before pinch-off. d_d^* is taken as the diameter of the separating droplet when the primary breakup mode is droplet, however when the primary breakup mode is a pinching jet it is measured across the "shoulder" of the downstream separating jet. See Figure 3.2 for illustration.	
d_j	jet exit diameter (taken as d_e)	
d_j^*	jet diameter measured in last frame before pinch-off. Measurement taken across last disturbance prior to necking.	
d_s	satellite droplet diameter	
FOV	Field of View – size of observable region for photographs	

Fr	Froude Number $= \frac{U_e\sqrt{\rho_i}}{\sqrt{\Delta\rho g D}}$
g	gravitational acceleration
l_a	maximum intact column length after breakup, approximately equivalent to distance from nozzle exit to location of breakup (pinch-off)
l_b	maximum intact column length the instant before breakup
l_c	intact column length at breakup length
l_n	neck length
LIF	Laser Induced Fluorescence
neck	Capillary
N_j	Buoyancy number $= \frac{U\rho_d}{\mu_d}\left(1-\frac{\rho_a}{\rho_d}\right)\left(\frac{\sqrt{(\rho_a-\rho_d)gd}}{U_e\sqrt{\rho_d}}\right)$
PIV	Particle Image Velocimetry
Re	Reynolds Number $= \frac{\rho_i U_e D}{\mu_i}$
We	Weber Number $= \frac{\rho_i U_e{}^2 D}{\sigma}$
We*	Weber Number based on pinch-off dimensions $= \frac{\rho_i (u_j{}^*)^2 d_j{}^*}{\sigma}$
u_e	nozzle exit velocity
u_j*	fluid velocity through jet calculated near pinch-off
VOF	Volume of Fluids method
Oh	Ohnesorge Number $= \frac{\mu}{(\rho D\sigma)^{1/2}}$

Greek

$\Delta\rho$	difference in density between ambient fluid and dispersed phase fluid
λ	viscosity Ratio $= \frac{\mu_d}{\mu_a}$
μ_d	jet fluid viscosity
μ_a	ambient fluid viscosity
ρ_d	jet fluid density
ρ_a	ambient fluid density
σ	interfacial surface tension
θ_u	upstream pinch-off angle
θ_d	downstream pinch-off angle

Subscripts

a	ambient fluid property
d	dispersed phase fluid property (also used to signify droplet/ downstream condition)
j	jet property
s	satellite property
u	upstream condition

Superscript

*	Pinch-off condition

Chapter 1

Introduction

1.1 Generalized Problem Statement

1.1.1 Background

The interaction of two fluids has been of interest to the engineering community for more than a century. The problem has traditionally been split into two major areas of study depending on whether the interaction is between a liquid and gas or between two different liquids. Most of the historical and recent literature focuses on the interaction between a liquid and a gas, but the two fluid interaction problem is gaining more interest as generalized solutions are sought.

Many industrial processes rely on liquid-liquid systems. Microencapsultion is an area of great current interest, particularly in the bio-medical arena. A liquid-liquid system can be used to entrain the ambient fluid within droplets of the working fluid, which has been shown to occur using the present experimental setup on multiple occasions. There is promise for using this technique to formulate pharmaceuticals or even to help with environmental cleanup such as removing oil from ocean waters.

Furthermore, inkjet printing technology is rampant as manufacturers try to improve resolution of their products. By understanding and quantifying the breakup and pinch-off

phenomena, controlled droplet sizes and volumes can be created by introducing electric fields or defined perturbations. The literature has shown that promising research is being performed to study how to suppress certain breakup modes as well as force a specific mode to occur for a liquid jet in air [Ganan-Calvo and Barrero, 1998]. Similar opportunities exist for a liquid-liquid system.

Little quantitative work was found on pinch-off dynamics, particularly on pinch-off in liquid-liquid systems. The published experimental data focused largely on downstream conditions such as mean droplet size [Merrington and Richardson, 1947 and Heertjes et al, 1971a, b], evolution of droplet size and shape [Zhang and Bassaran, 1995], surface topology [Cohen et al. 1999 and Chesnokov, 2000], satellite behavior [Pimbley and Lee, 1977], satellite formation [Tjahjadi, 1992], maximum column length [Tyler and Richardson, 1925, Meister and Scheele, 1969a and Richards et al, 1995], and atomization [various]. The pinch-off phenomenon itself was scarcely dealt with and what has been published deals almost exclusively with liquid-gas systems.

1.1.2 Problem Statement

The present study focuses on capturing and quantifying the breakup and pinch-off of a liquid jet when injected into a second, immiscible liquid. A nozzle with a 97 μm opening is used to generate a jet of 53.4% Water-Glycerin (by weight) flowing into an ambient fluid of Clearco Pure Silicone Fluid 50. The breakup mode is studied for a range of Reynolds, Weber number combinations by varying the jet exit velocity. The range of interest is from near the onset of Rayleigh type breakup up to and including the transition to sinuous breakup.

Key metrics are the upstream and downstream cone angles, breakup location, breakup modes, separating droplet diameters, and the ratio of the forming droplet diameter to the maximum disturbance diameter just before pinch-off. The upstream and downstream cone angles are often referred to as jet and droplet pinch-off angles, but the present study shows that above a certain We number the jet pinches off into a second jet and the separating fluid is not a droplet but rather still in the form of a jet. The second jet is naturally unstable and would in turn break down forming multiple drops. For this reason, it is believed that the use of the terms jet and droplet cone angles is inappropriate.

1.2 Previous Studies

The study of liquid jets first became prominent with the work of Rayleigh (1878). He argued that jet instability was the result of one of two causes; dynamic breakup or capillary forces. His original work reviewed Plateau (1873) and Helmholtz (1868), going on to develop equations to predict the dynamic and capillary breakup of these liquid jets. Rayleigh is generally credited with being the first to seriously study an inviscid jet breaking up in air.

Rayleigh followed this work with a more in depth study of the capillary breakup mode. He followed the 1878 investigation the next year by investigating high-pressure water flow through a circular orifice in a thin plate, creating a circular jet. In this work by Rayleigh (1879), jets that flowed horizontally through orifices of different shapes were studied. He found that the wavelength of the disturbance (defined as departure from

circularity of the jet) in the capillary is directly proportional to the square root of the pressure. This relationship holds well for low-pressure flows, but he found it necessary to develop a correction factor for higher-pressure streams. Rayleigh also studied the effect of introducing an electrical field to the jet. He found that the behavior of the droplets after pinching off from the main jet can be influenced to force droplets to coalesce, to force droplets to collide and bounce off of each other or to make the droplets miss one another all together.

Tyler is generally considered the first to increase the complexity of the pinch-off problem by adding viscosity into the study. He published a series of papers between 1925 and 1933 that studied a viscous fluid breaking up. His work [Tyler and Watkin, 1932] was the earliest work obtained that specifically investigated a liquid-jet breaking up in a second immiscible liquid. The major focus of this series of studies was on the breakup length of the liquid column and several characteristic curves were published for various liquid and air systems as well as liquid-liquid systems. The conclusion of this series of studies was that upper and lower critical velocities exist that correspond to maximum and minimum column lengths, respectively. The upper critical velocity corresponding to the maximum column length has subsequently been used as the transition point between varicose and sinuous breakup while the lower critical velocity corresponding to the minimum column length has since been considered to be the point or transition from dripping to jetting. Dripping is considered to occur when the fluid stream breaks into droplets at the nozzle exit without the formation of a stable liquid core. No general theory governing the breakup length was produced.

Meister and Scheele are cited most frequently in the field of liquid-liquid breakup. They published a series of papers beginning in 1967 that studied 15 mutually saturated liquid-liquid systems and primarily looked at breakup length and drop volume. They performed both experimental and theoretical work to try to refine classical models and develop empirical equations to predict droplet volume and column breakup length. The theory that was developed was in large part similar to the general theories presented by Tomitika (1934) and Tyler (1932, 1933).

Later studies of liquid jets began to look more closely at liquid-liquid systems. Gospodinav et al. (1978) developed an exact solution for velocity profiles of laminar jets in immiscible liquid-liquid systems. They employed a finite difference scheme to overcome some of the problems with earlier numerical solutions (see Duda and Ventris, 1967). Their results are compared to known experimental results [Yu and Scheele, 1975]. The biggest discrepancy between the numerical and experimental results takes place at the interface. This is likely due to the difficulty of adequately capturing and describing the interface with a limited number of grid points.

Further numerical investigations have been presented by Razumovski (1993). This work investigates Rayleigh's capillary breakup studies. A temporally periodic solution is obtained for the connected jet from the point of separation to the instantaneous position of the end of the jet. Surface tension and viscosity are included in the study, which is likely a contributing factor for the strong correlation between these results and the

experimentally observed profiles of Pimbley and Lee (1977) and others. Razumovski (1993) further explores the creation of satellite drops, separate from the large main drops. He uses numerical methods to describe the jet profile in the immediate region of the breakup. This differs from earlier works which were based on one-dimensional flow equations that neglected the radial dependence of the flow velocity. Near the breakup, the small perturbation approximations that had traditionally been used are in actuality no longer small, so the previous solutions were inaccurate. The flow near the breakup point determines the satellite type (neutral, fast or slow), which can be shown to be dependent upon jet length. Rayleigh's initial work (1878) can be used to accurately predict satellite formation for large Weber numbers, but provides no insight as to which type of satellite might be formed.

More recent studies of drop formation at the tip of a capillary tube immersed in another immiscible liquid have been performed by Zhang and Stone (1994). The boundary integral method was used for this numerical investigation for low-Reynolds-number flows. They have shown that for large viscosity ratios, λ, breakup occurs very quickly. There is no detectable thread between the outlet and the droplet, and no satellite droplets are formed. As λ increases, a thread forms between the outlet and breaking droplet. The distance to detachment changes significantly when $\lambda > 1$, but the volume of the droplet varies little. Several parameters were varied during this study, including the Capillary number, *Ca*, the Bond Number, *Bo* and viscosity ratio. The viscosity ratio is found to have a significant effect on satellite formation, increasing the thread length between droplets as λ goes up. This effect is ever more evident when $\lambda > 1$. The formation of

satellite droplets is shown to be directly related to the viscosity ratio as well. Satellite droplets begin to form at $\lambda = 0.1$ and increase in size with increasing λ. The drop volume is not fully dependent on λ, but a strong correlation is shown between drop volume and Bond number, *Bo*. The primary drop volume decreases nearly linearly with *Bo*. The secondary, satellite droplet takes longer to form and is relatively larger as *Bo* increases. The Capillary number is shown to drive the breakup time

Kowalewski (1995) performed an in depth experiment which studied the separation of droplets from the liquid jet. This study was limited to a liquid jet in air. The details of the thin thread connecting the droplet to the jet just before separation were investigated as well as the shape of the pinch-off region. Viscosity of the liquid was shown to have a strong effect on the shape and length of the neck (the region where the droplet begins to break off and where it finally detaches), however the diameter of the neck did not seem to vary significantly before breakup regardless of the viscosity of the liquid.

Most studies have neglected the pinch-off region due to the small scale of the detachment zone. Kowalewski (1995) employed modern imaging techniques to capture the jet tip near separation in order to compare what he observed to the predictions of Eggers' (1993) model. Jets ranging from 50 to 900 μm radii were forced downward into air. The breakup of the jet was forced by applying a controlled disturbance to the system, with typical breakup length 100-200 times the jet radii. The effects of the surrounding air and gravity are considered negligible.

Kowalewski (1995) concludes that the thread diameter just before droplet formation is generally on the order of 1μm, and also that this is probably the limiting diameter for the thread just before the droplet separates. Two main phases of the breakup process are identified; the main jet begins to neck close to the droplet surface, which continues to thin until a micro-thread is all that connects the droplet to the main jet and then the continued thinning of the micro-thread due to flow back to the macro-thread slows down. The slow down of the flow from the micro-thread causes a pressure difference, which in turn begins to pull on the micro-thread causing it to elongate further. The experiments were able to show that Egger's (1993) model can be used to find the maximum length of the micro-thread and the variation of the thread diameter before pinch-off, but does not adequately predict the final thread diameter, the point of the pinch-off or the thread retraction velocity. Kowalewski's (1995) final conclusion was that the pinch-off process seems to be insensitive to the external initial conditions, diameter or perturbation amplitudes.

Webster and Longmire (2001) performed detailed experiments on the effect of viscosity ratio and forcing frequency on drop size, pinch-off angles, number of drops and spacing. Jet pinch-off was forced by inducing a controlled disturbance into the flow. Varying the frequency of the disturbance (and thus, the Strouhal number, St) forced the break up of the jet to occur at a specific location. By controlling the location of the jet break up, investigating physical characteristics of the phenomena became much easier. They were able to capture multiple images of the break up at specific times, which allowed the use

of several different occurrences to determine common characteristics. Laser Induced Fluorescence (LIF) was used to capture all images for this work.

LIF uses a fluorescent sensitive pigment injected into one fluid so that the two fluids can be discerned from one another when photographed under fluorescent lighting. By taking high-speed photographs, Webster and Longmire (2001) were able to measure certain physical characteristics of the break up zone. As shown in Figure 1.2, the angle formed by the retracting jet and separating droplet could be measured, as well as the droplet shape, spacing and downstream speed. This was done for two different fluid combinations over a range of velocities. The properties of the fluid combinations studied were very similar, except that the second fluid combination had a much higher λ.

The less dense fluid combination showed a much higher sensitivity to the Strouhal number. By changing only the forcing frequency, the size and number of drops separating from the jet within the region of interest could be changed from zero at higher frequencies to several droplets at lower frequencies. The jet itself could even be seen to have a wave-like shape just before break up (see Figure 1.3).

The viscosity ratio of the jet fluid to the ambient fluid has a direct effect on the jet behavior. The larger viscosity ratio fluid combination produced larger droplets after breakup that were less sensitive to changes in *St*, and smaller interface angles between the jet and droplet were observed. The natural, unforced flow for the higher viscosity fluid combination also broke up much more quickly than did the lower viscosity fluid

combination, but higher flow velocities tended to remain unseparated (also opposite of lower viscosity behavior).

Further work by Longmire et al. (2001) built upon the initial work by Webster and Longmire (2001). They studied the dynamics of pinch-off in liquid-liquid jets with surface tension. These experiments used the same fluid systems to study velocity and vorticity distributions within the flow. Particle Image Velocimetry (PIV) was used to capture the internal structure of the flow, while LIF was used to capture the full jet structure. The PIV system works by shooting a double-pulsed laser into the flow, which has seed particles embedded into it. The laser reflects from the seed particles and the camera captures the images for processing by a computer. According to the paper, results of this analysis agreed well with Zhang and Lister (1999).

Differentiating the results of the velocity profile, the internal flow vorticity was also studied. Again as in the previous work by Webster and Longmire (2001), the viscosity ratio was shown to have a significant effect on drop formation and separation as well as the resulting droplet shapes. The lower viscosity ambient fluid showed greater effect on gravitational acceleration for the droplet than the higher viscosity ambient (as could be intuitively expected), which in turn resulted in smaller droplet and jet diameters.

The higher viscosity ambient had a damping effect on droplet oscillations after pinch-off. The droplets in higher viscosity ambient maintained a spherical shape throughout the region of interest, while the droplets flowing in the lower viscosity ambient fluid

oscillated forming an inverted curvature on the upstream side with a cusp at the location of the largest diameter. These results provide good experimental data for future numerical models of jet formation and pinch-off for two immiscible liquids with surface tension by analyzing the internal flow structure.

Milosevic and Longmire (2002) expanded this work in order to classify the different modes of pinch-off and study satellite droplet formation. Satellites are considered to be smaller, secondary droplets that separate from the initial main droplet. A similar fluid system was used for this experiment compared to the two earlier studies. PIV and LIF were again employed, but the region of interest was reduced for this study.

Results from this study indicate that there is a direct, observable dependence of satellite formation on St, but no convincing dependence on Reynolds number could be found. Satellite formation was generally associated with lower Re and St. Interface shape as pinch-off occurred as well as the internal flow field (velocity gradients) also play an important role in the formation of satellite droplets.

More recently, attention has been given to micro-jet breakup analysis. Vago et al. (2003) presented a new technique for visualizing this breakup, which they deem the light-guided method. An investigation into the phenomena of jetting and breakup was not presented, only measurements showing this new technique is as good or better than high-magnification, high-speed shadowgraphy.

Further studies of micro-jets have begun, but little experimental work has been published. Ho et al. (1999) presented a non-dimensional grouping comparison coupled with a numerical model that studied variations of Capillary and Ohnesorge numbers. This numerical study used the dimensionless groups to determine which ones could be used to force a stable flow. It is included only to impress upon the reader how much there is to do on the study of micro-jets. Ho et al. (1999) used the numerical simulation of a micro-jet (microscale concentric flow is the term they use) to make determinations that have been well known for macro-scale flows and argue the key to forming a stable micro-jet is to maintain the Capillary number greater than unity.

The works discovered that specifically addressed the issue of beginning with a micro-sized exit and an expanding jet were those published by Das (1980, 1989 and 1997). All previous work has assumed a constant diameter jet or a contracting jet [Meister and Scheele, 1969a]. Das (1997) also broke from traditional theory, reporting that the jet diameter at breakup was the most important physical parameter in determining the size of separating droplets. The other authors surveyed based their evaluations and calculations on the exit geometry and fully ignored the geometry at the breakup point. Das (1997) also reports that jet contraction or expansion had not previously been confirmed and describes a model predicting jet expansion whenever drag forces on the jet surface due to continuous phase viscosity exceed the buoyancy and momentum forces [Das, 1997].

The literature has almost exclusively focused on jetting phenomena at the macro scale, and even more so on breakup length, droplet volume and satellite formation. Some work has looked at the diameter of the capillary thread just before pinch-off [Kowalewski, 1995] and at the size of satellite droplets but there is little information on what effect beginning with a liquid jet on the micro scale would have on this classical problem. New technologies and increased environmental regulations have increased the importance of this investigation. Inkjet printer technology, industrial scrubbers and other applications where increased droplet surface area is desired for heat or mass transfer are all sectors which could benefit from this study.

1.3 Specific Objectives

The goals of this thesis are to experimentally investigate the pinch-off of liquid jets flowing in a second immiscible liquid with a jet exit diameter on the micro-scale. This work will examine the breakup length, droplet diameters, upstream and downstream cone angles when pinch-off is eminent, neck length just before pinch-off, and droplet to jet diameter ratios for a range of Reynolds and Weber numbers.

1.4 Organization of the Thesis

This thesis is organized into four chapters and one appendix. The first chapter, which has already been presented, describes previous work in the area of liquid-jet breakup and sets the groundwork and objectives for the rest of this work. The second chapter describes in detail the experimental setup and procedures. Results follow in the third chapter with concluding remarks and recommendations for future work following in the

fourth. The appendix presents the data used to develop all graphs and tables.

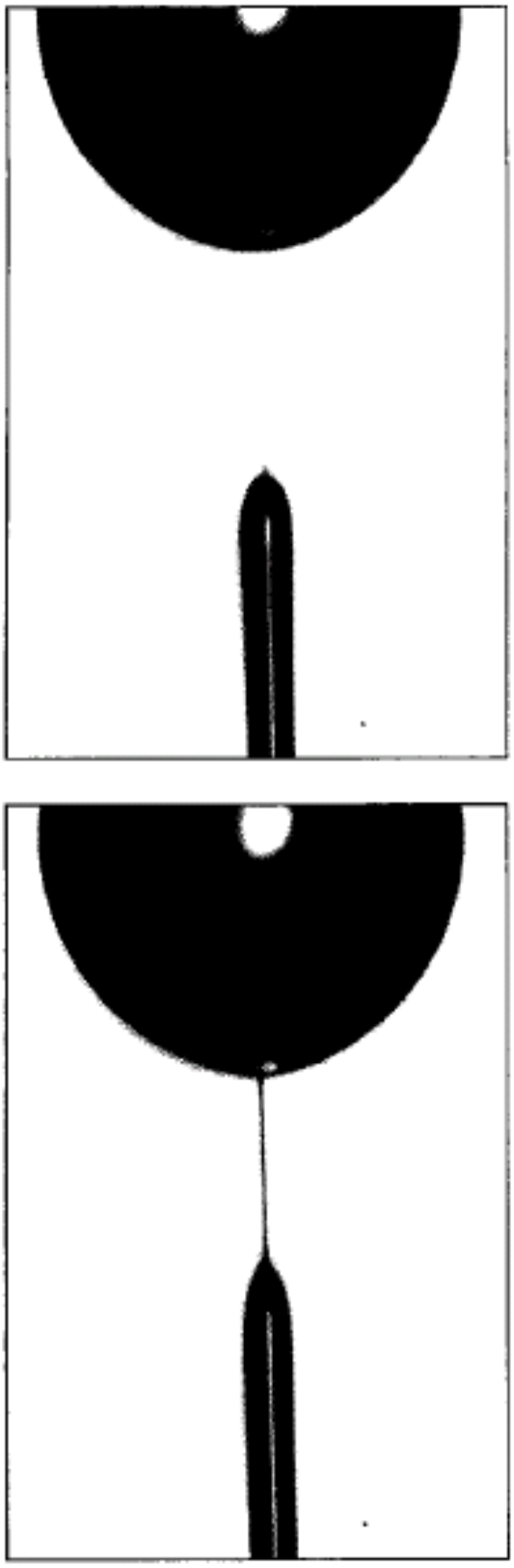

Figure 1.1 Photo showing thin filament between neck and detaching droplet [Kowalewski, 1996].

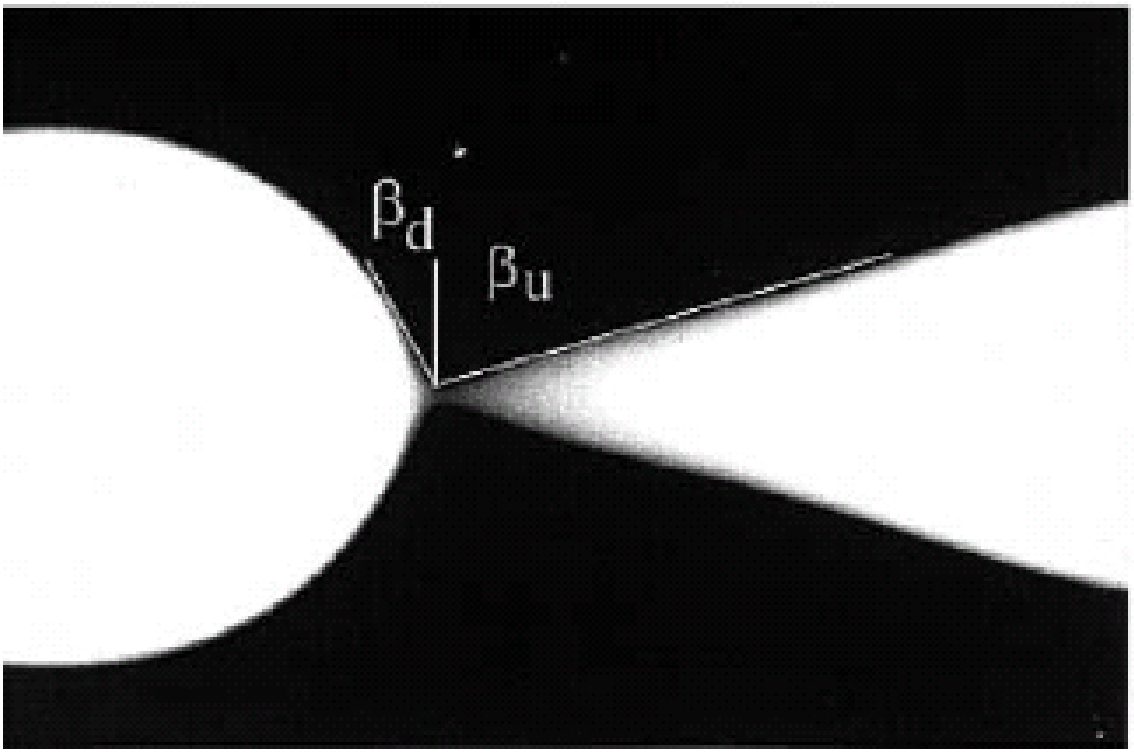

Figure 1.2 Historical definition of jet and droplet pinch-off angles [Webster and Longmire, 2001]

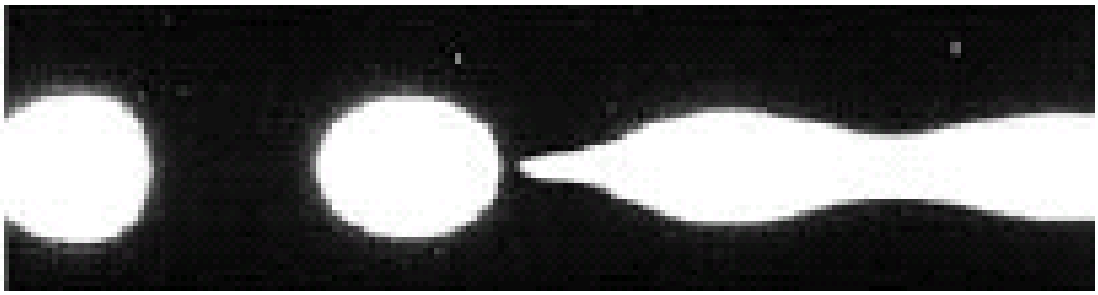

Figure 1.3 Wave-like shape of jet just before breakup [Webster and Longmire, 2001] for St= 3.1, Re = 50, and Fr = .26.

Chapter 2

Experimental Method

2.1 Introduction

This chapter will introduce the equipment and methodology used to carry out the present experimental investigation.

2.2 Test Apparatus

An open loop system was employed to force the working fluid through a 97 μm nozzle into a viscous ambient of 99.9% pure silicone fluid (Dimethyl Polysiloxane). The collection tank used for this experiment was a tall glass cylinder with a diameter of 14 cm and height of 50 cm. A high-speed digital camera with a 512 X 512 CMOS sensor (IDT XS-4 Camera) was used to capture images at frame rates from 5000 fps when using the full sensor image and up to 31,500 fps when reducing the region of interest on the sensor to less than 512 lines. The camera was equipped with a 60mm Nikor lens attached to a Nikon PB-6 bellows, which was used to obtain the high magnification necessary to view these phenomena.

The working fluid was dyed with a small amount of red food coloring (less than 0.2% by weight) to provide contrast between the working fluid and ambient fluid so that the interface between the two could be observed. A 500W halogen lamp was used to provide backlighting (slightly off center) along with a diffusive screen between the

halogen lamp and collection tank. A small fan was placed perpendicular to the setup which forced air around the tank and over the halogen lamp to keep the fluid in the tank from heating up. With the halogen lamps placed 1.0 m from the tank, no change in fluid temperature was observed when the fan was used. The camera was placed on the opposite side of the tank from the halogen lamp so that the edges of the jet and subsequent droplets would show up clearly on the digital camera.

The dispersed fluid (see Table 2-1) was forced through the nozzle by pressurized nitrogen gas. An aluminum honeycomb baffle was placed into the piping system between the gas outlet and fluid inlet to reduce the velocity of the gas. This prevented nitrogen from penetrating and dissolving in the working fluid. Additionally, a 7 μm in-line filter was used between the fluid inlet and nozzle exit to help prevent the nozzle from becoming blocked by small particles. System pressure was controlled through the use of a 0-600 psi pressure regulator at the Nitrogen tank outlet. The pressure was checked and recorded just upstream of the nozzle to help ensure consistent exit conditions were maintained. The pressure gauge was an Ashcroft Duralife 0-200 psi gauge with ±1% accuracy and 2 psi graduation. Figure 2.3 shows a sketch of the experimental apparatus.

2.3 Instrumentation and Measuring Techniques

A calibration image was taken every time the camera set up was changed or moved. To ensure the calibration image was taken at the correct working distance from the camera lens, a small droplet of working fluid was allowed to collect at the nozzle exit. The

camera was then focused on the droplet to establish the correct camera/lens location and focus. A scale was then inserted into the ambient fluid and placed against the nozzle exit so that it would slice through the small droplet of working fluid. The calibration image was then taken. All calibration images were measured in a region outside of where the droplet was located in order to keep the droplet from distorting the calibration measurements.

In order to ensure that the curvature of the large diameter collection tank did not distort the images in the horizontal direction, a calibration image was taken and measured in both the horizontal and vertical directions. Some distortion did occur, but due to the large diameter of the tank and comparably small diameter of the jet and escaping droplets, this distortion was found to be minimal. Because the distortion was less than 1%, it was determined that the calibrations would only be made in the horizontal direction.

Computer software (SigmaScan Pro 5.0) was used to measure pinch-off angles of droplets and the cone of the jet as well as jet and droplet diameter. Additionally, the diameter of the thin capillary connecting the neck of the jet and the escaping droplet was measured when possible (however these measurements are not reported, as the minimum neck diameter should reduce to zero at pinch-off). The jet velocity was determined by using SigmaScan to calculate the volume of individual droplets and then calculating the exit velocity based on the nozzle diameter and volumetric flow rate. The droplet volume was determined by using the volume of an ellipsoid because the diameter in the streamwise direction was not the same as that perpendicular to the flow. This is a small

improvement over the assumptions made by Meister and Scheele (1967a) and Christianson (1955), who used the volume of a sphere based on the mean diameter of the major and minor axes combined. Christianson concluded that if the major axis to minor axis ratio was less than 1.7, the droplet volume calculation (assuming a spherical droplet) would be less than 5% in error. The droplet axis ratio that was observed for this experiment was consistently below 1.26. Figure 2.4 shows how the cone angles are measured as well as the definite change in both upstream and downstream angles immediately after pinch-off. The top photograph in Figure 2.4 shows the moment just before pinch-off while the bottom image shows the photograph one frame later, just after pinch-off occurred (which is consistent with Eggers' similarity solution [Eggers, 1997]. All images were searched thoroughly to ensure the photo just before pinch-off was used and not the photo just after pinch-off. This was done by using the computer to look at the photographs in quick succession, which created a slow-motion movie. By watching the images in slow motion, changes in shadows and geometry in the necking region could be observed which were not noticeable if viewing the images one at a time.

Previous works [Rayleigh, 1878, 1879, Webster and Longmire, 2001, Meister and Scheele, 1969, etc.] have assumed jet symmetry. This assumption allowed previous authors to simplify their measurement of the cone angles as it is difficult to use the center of the jet as the measurement reference plane. However, as shown in Figure 2.6, the jet may not be symmetrical due to sinuous disturbances causing jet disintegration. Since the jet is obviously not symmetrical at all conditions, the full cone angle of the jet

and separating droplet should be measured as opposed to measuring with respect to the vertical or horizontal planes as has been done previously [Longmire and Webster, 2001].

The field of view was varied in order to observe different aspects of the breakup phenomena. When the pinch-off dynamics and geometry were to be measured, a small field of view (around 2.5 mm X 2.5 mm) was used. This was further reduced in one direction (parallel to fluid flow) for high-speed imaging. In order to view and characterize the different breakup modes, a larger field of view was used (up to 48 mm X 48 mm). When a field of view was used that was large enough to capture both the nozzle exit and the breakup location, the resolution of the images was too poor to observe the small details of the breakup location, such as satellite formation and cone angles. Figure 2.7 is included to demonstrate how large the field of view must be in order to measure the breakup length. Figure 2.7 also shows very clearly that the jet diameter expands upon exiting the nozzle, which was also observed by Agnew et al (1982), Das (1989, 1997) and Koob and Hill (1985). For Figure 2.7, the 18 mm field of view (FOV) corresponds to 35 μm per pixel, so the 97 μm exit is just barely resolvable at this FOV. Additionally, for the smallest fields of view, drop diameter measurements were limited to approximately 20 μm with measurement uncertainties of plus or minus 1 pixel due to the resolution of the camera. For a 2.5 mm field of view, each pixel represents 5 μm and it is assumed that two pixels are required to define the drop.

In order to determine the importance of gravitational effects, the Bond number, Bo, was calculated. The Bond number is a measure of the importance of gravitational effects relative to surface tension effects and is defined as

$$Bo = \frac{g \cdot (\rho_d - \rho_a) \cdot d_e^{\,2}}{\sigma} \qquad \textbf{(2.1)}$$

where g is acceleration due to gravity, ρ_d is the density of the working fluid, ρ_a is the density of the ambient fluid, d_e is the nozzle exit diameter and σ is interfacial surface tension [Longmire and Webster, 2001]. For the present study, Bo is 5.62E-4 based on nozzle exit diameter. Bo this small suggests that gravitational forces are negligible for this experimental setup. Bo is also based on the droplet diameter [Liu, 2000] rather than the nozzle exit diameter. For this reason, the diameter of the largest droplets were also used to verify that Bo for the droplets is small. The Bond number based on the largest droplet (measured far downstream of the pinch-off location) is 0.53, which suggests the surface tension effects are comparable to gravitational effects for large separating droplets.

To further confirm that the effects of gravity could be neglected in most cases, the Froude number,

$$Fr = \frac{U_e \sqrt{\rho_d}}{\sqrt{\Delta \rho g D}} \qquad \textbf{(2.2)}$$

[Linden, 1973] was also studied. Froude number is a measure of the inertial forces to gravitational forces. For the present study, the length scale used was the orifice

diameter. This yielded Fr ranging from 143 to 1343 which is much greater than 1 in all cases.

There are several dark spots on many of the photographs. These are due to dust on the CMOS sensor and are not aberrations in the flow or dropped pixels (pixels that were not recoded by the camera or transferred to memory from the camera) (see Figure 2.6). After several days of testing, the ambient fluid had collected dust particles which begin to show up on some of the high speed images. These dust particles are assumed to have negligible effect on the flow dynamics as no changes in the flows were observed between the initial images taken with clean fluid and the images taken at the end of the study where the fluid had the most dust accumulation. .

2.4 Test Conditions

A 53.4% Water-Glycerol jet was forced into 99.9% pure Silicone Fluid (Dimethyl Polysiloxane) using compressed Nitrogen gas. The solution percentage of water and glycerol was determined by matching the index of refraction of the dispersed and ambient fluids [Webster and Longmire, 2001].

Experiments were performed at room temperature (22.2 – 25.5° C). The jet was forced by compressed nitrogen gas at pressures ranging from 0 – 1100 kPa. Only inlet pressure was varied to change the jet exit velocity. Due to the possibility of the filter becoming partially blocked and affecting the discharge velocity, images were taken at locations far downstream of the initial breakup and analyzed to determine the volumetric flow rate.

This was done for each test condition. It was found that the discharge velocity did change over time for the same inlet pressure, so it was not possible to use the inlet pressure for anything more than a reference point. A pressure gauge was installed downstream of the filter in order eliminate errata caused by the filter becoming blocked.

Data was taken for thirteen different exit conditions and also recorded at the pinch-off location. Almost all data in the literature [Meister and Scheele, 1969a, b, Tyler 1932, 1933, Webster and Longmire, 2001, etc.] was referenced to the nozzle exit condition, but due to the unique problem of an expanding jet, the jet diameter at the exit was not representative of the jet at pinch-off. For this reason, the conditions at pinch-off were used whenever the parameter of interest was near the pinch-off location, which is similar to Das (1997). Table 2-2 and Table 2-3 list the range of test conditions observed in the small field of view study in the pinch-off region. Furthermore, the Ohnesorge number was held constant for the range of experiments performed in this study (Oh = 0.138).

2.5 Experimental Procedure

Figure 2.5 (upper) illustrates a pure distilled water jet issuing into the Dimethyl Polysiloxane fluid, which shows the system when the working fluid's index of refraction does not match that of the ambient. The lower image shown in Figure 2.5 illustrates the 53.4% water-glycerin mixture with the index of refraction matched to the ambient.

High-speed photographs were taken at frame rates up to 31,500 fps. Figure 2.7 shows a representative photograph of the jetting fluid leaving the nozzle exit. The diameter of

the jet just past the exit was measured to be 99 μm, or within 3% of the manufacturer's published orifice diameter of 97 μm. Figure 2.7 also shows that the jet expands after exiting the orifice. The jet has expanded to 3.2 times the exit diameter (322 μm) by the time it travels 44 diameters downstream. The jet was observed to remain intact at over 100 times the exit diameter downstream for some test conditions.

The data has been reduced in order to report the 95% confidence level. The Student's t-distribution chart [Crow et. Al, 1960] was used to determine the range in which 95% of all experimental data is expected to fall. The table that was used is one-sided, meaning that 95% of all data points are expected to fall below or above the calculated values. For this reason, the 97.5% confidence level table was used in both directions in order to establish the 95% confidence level band. All experimental uncertainties were calculated with 95% confidence level (Crow et al, 1960).

The key distinguishing features of the present study compared to Meister and Scheele (1969a, b), and others in the literature are the consideration of the expanding jet seen in the present study as well reporting of observations taken at the pinch-off location. Previous works have referenced all measurements and governing equations to the nozzle exit, which is appropriate if the jet maintains a constant diameter after leaving the nozzle. However, if the jet expands or contracts, using the nozzle exit conditions are not appropriate as the diameter of the jet near pinch-off may be different than the diameter of the orifice by an order of magnitude or more. For this reason, it is proposed that all measurements and observations regarding breakup phenomena should be

referenced to the region of the jet pinch-off rather than to the nozzle exit. The present study reports data in terms of the pinch-off conditions (i.e. the diameter of the jet and separating droplet at pinch-off rather than downstream of the pinch-off location) with the exception of the breakup length, which required a larger FOV.

Table 2-1 Fluid Properties

Fluid	μ (cP)	ν (cS)	ρ (kg/m^3)	n_d	σ *(mN/m)*
53.4% Water/Glycerol Mixture	7.3	6.4	1135	1.403	29
Clearco 50 Pure Silicone Fluid	48	50	960	1.403	

Table 2-2 Jet Exit Conditions

V (m/s)	Re	We	Fr	Ca
1.73	27	11	143	0.44
4.23	64	68	348	1.06
5.05	76	97	416	1.27
5.94	90	134	489	1.50
6.21	94	146	511	1.56
7.00	106	188	577	1.76
7.79	118	233	642	1.96
8.19	124	254	674	2.06
10.94	166	456	901	2.75
11.17	169	475	920	2.81
11.69	177	518	963	2.94
12.02	182	553	990	3.02
12.28	186	596	1012	3.09
12.54	190	603	1033	3.16
13.41	203	685	1105	3.38
13.60	206	705	1120	3.42
15.91	241	961	1311	4.01
16.31	247	1013	1343	4.10

Table 2-3 Pinch-Off Conditions

We	u^* (mm/s)	Re^*	We^*	Fr^*	Ca^*
11	32.82	4	0.030	0.68	0.008
68	67.08	8	0.136	5.53	0.017
97	95.13	12	0.287	0.80	0.024
134	103.68	12	0.310	8.54	0.026
146	93.68	12	0.272	7.72	0.024
188	73.15	11	0.200	6.03	0.018
233	69.89	11	0.197	5.76	0.018
254	99.32	14	0.341	8.18	0.025
456	126.07	18	0.564	1.94	0.032
475	189.41	22	1.050	4.12	0.048
518	88.65	15	0.341	7.30	0.022
553	109.98	17	0.476	9.06	0.028
596	128.44	19	0.612	10.58	0.032
603	198.04	24	1.192	16.31	0.050
685	145.93	21	0.778	2.45	0.037
705	190.50	24	1.169	15.69	0.048
961	269.10	31	2.121	22.17	0.068
1013	206.76	28	1.450	17.03	0.052

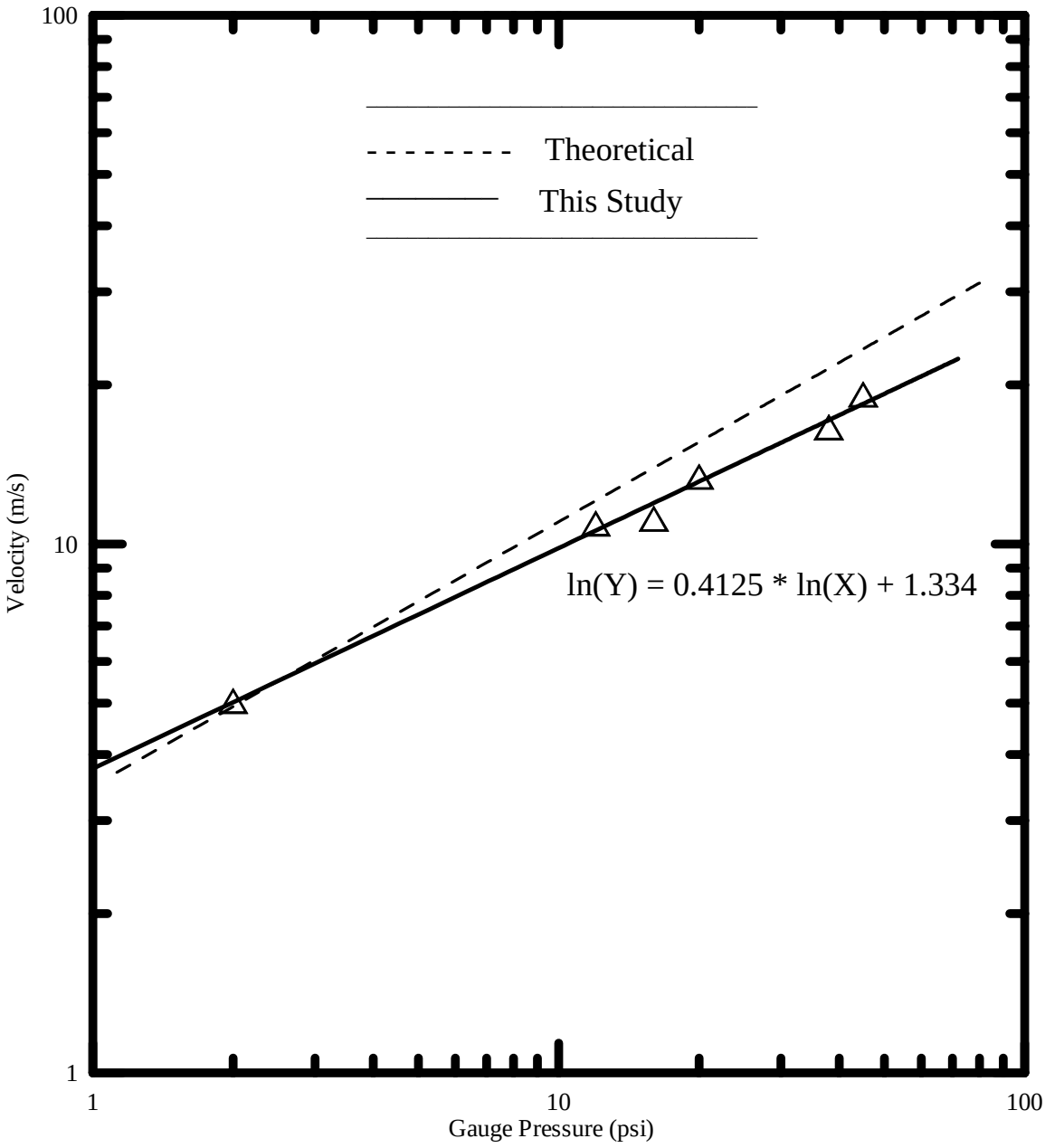

Figure 2.1 V**elocity calibration based on gauge pressure near nozzle exit.**

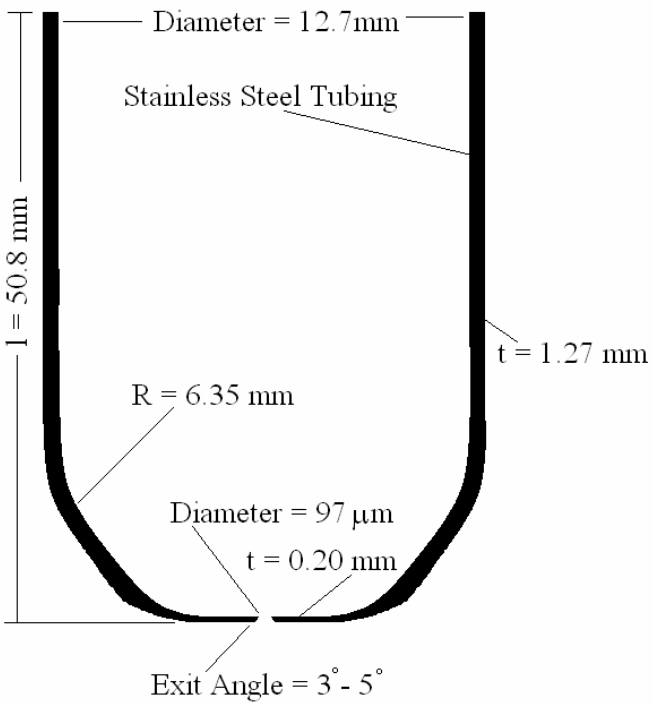

Figure 2.2 Nozzle geometry.

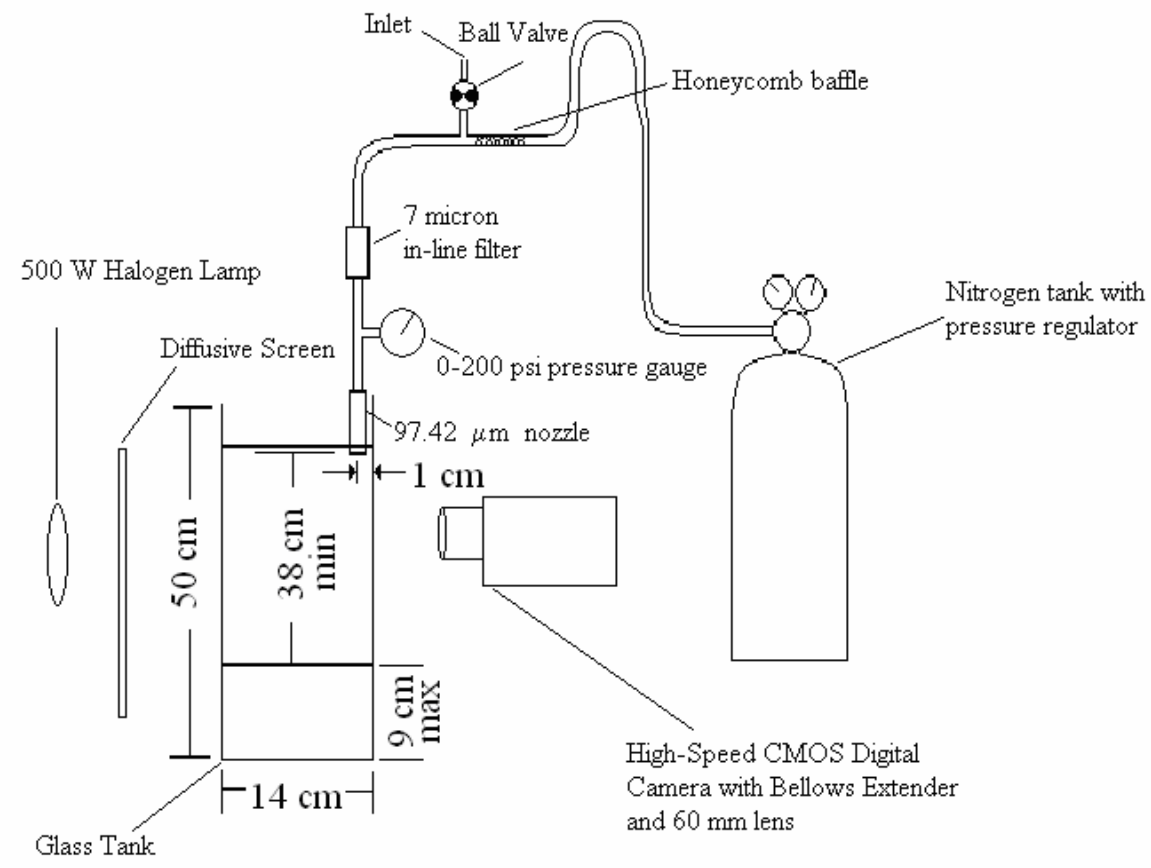

Figure 2.3 Experimental Setup

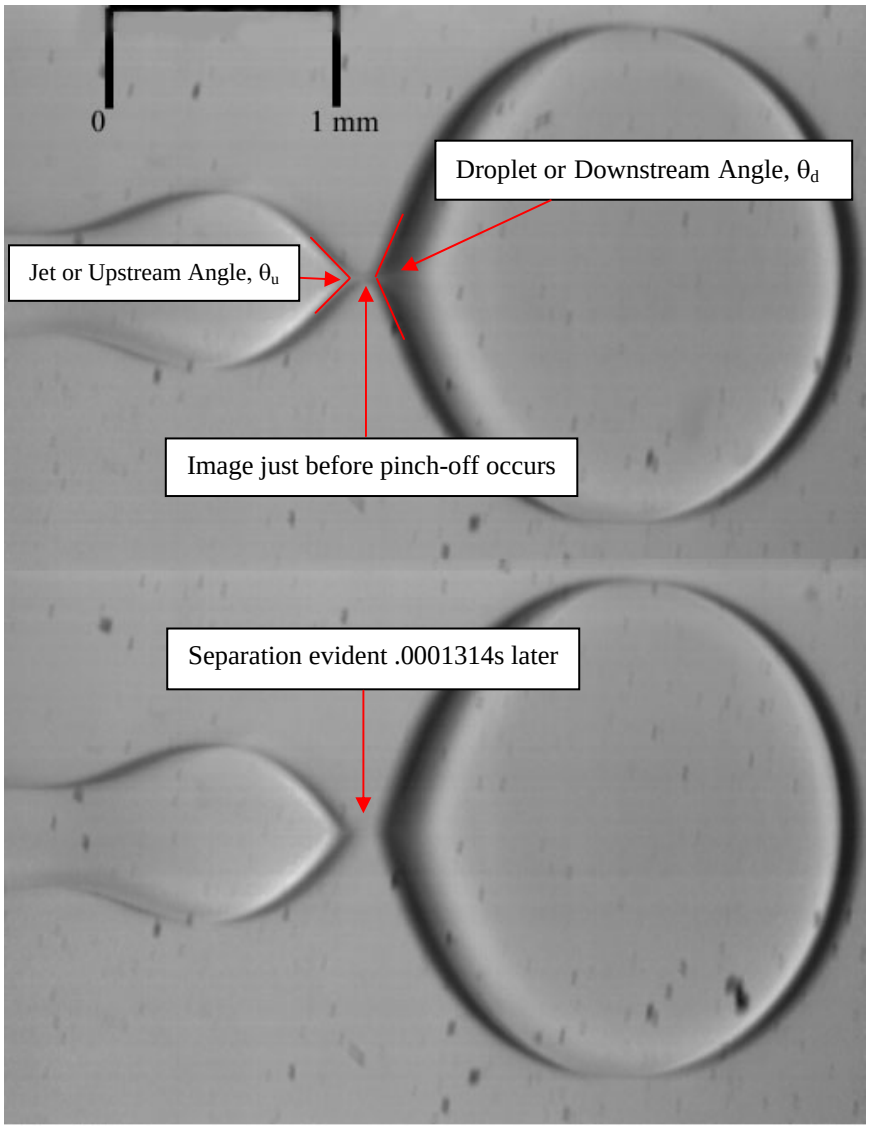

Figure 2.4 Pinch-off measurement configuration.

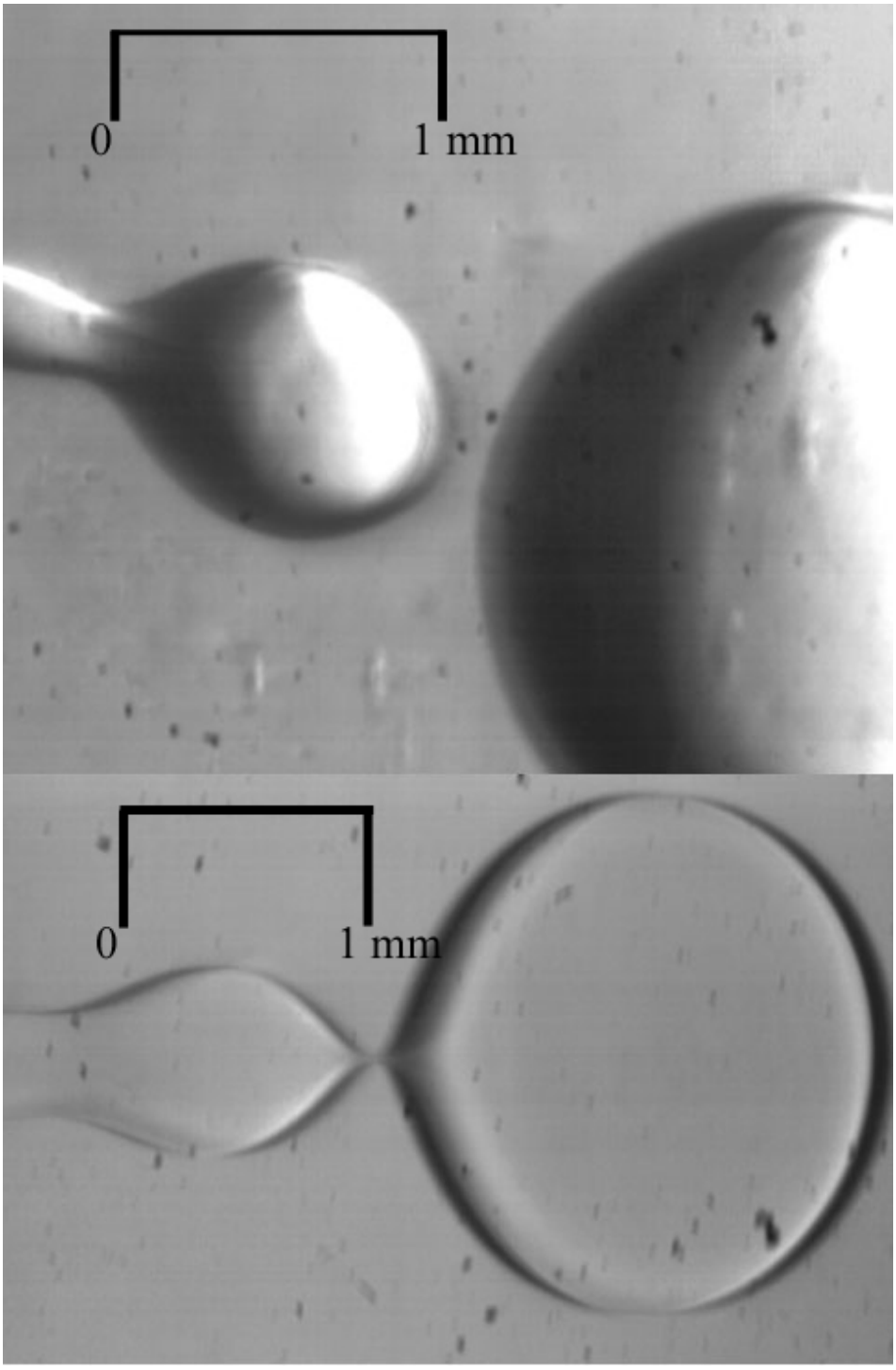

Figure 2.5 Upper image shows water injected into ambient silicone fluid. Lower picture shows 53.4% Water-Glycerin mixture injected into pure silicone ambient.

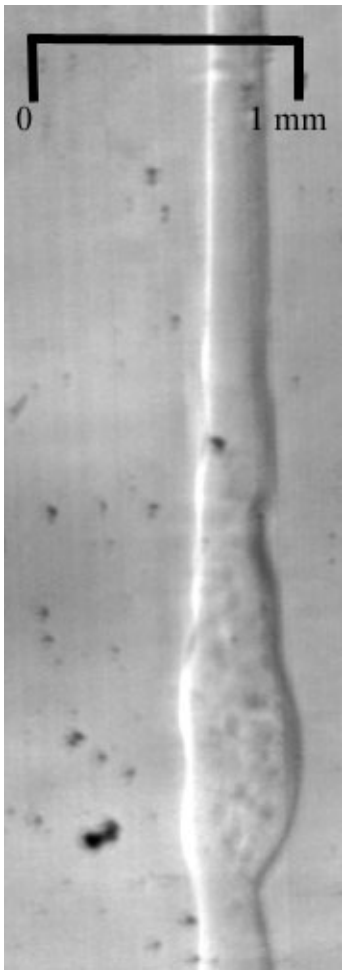

Figure 2.6 Flow Asymmetry seen at Re = 241, We = 961. 53.4% Water-Glycerol mixture in 50cSt Silicone Fluid.

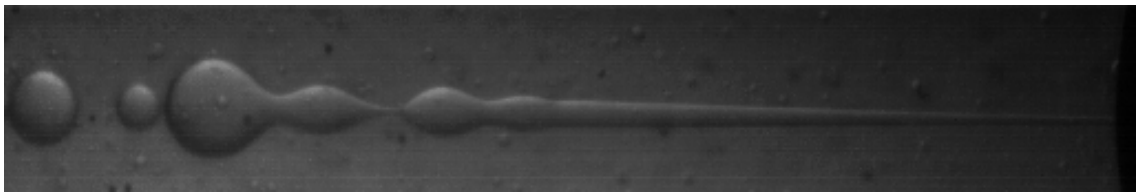

Figure 2.7 Jet at Nozzle Exit. Jet expansion clearly shown. Length of jet from nozzle exit to edge of image is 18mm (180 d_{jet}). 53.5% Water-Glycerol Mixture in 50 cSt silicone fluid, injected vertically downward. Image shown for Re = 170 , We = 475.

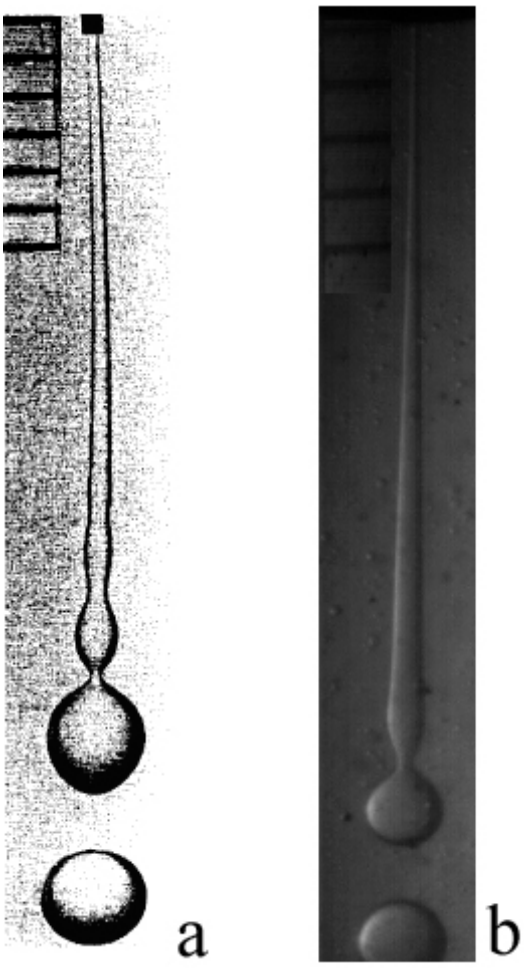

Figure 2.8 a) Das (1997) *D* = 0.255 mm U_n = 1.4 m/s Water in Paraffin. b) Present study *D* = 0.100 mm U_n = 11 m/s Water-Glycerin mixture in Silicone Fluid. Scales show 1mm increments for both images.

Chapter 3

Results and Discussion

3.1 Introduction

As stated earlier in Chapter 1, the expanding jet of the present study dictates that conditions at breakup govern the behavior of the pinch-off phenomena. Peregrine et al. (1990) were the first to explain that the dynamics near breakup are independent of the particular setup (initial conditions) such as a dripping faucet for example, causing the breakup to be localized both in space and time. A new definition of the Weber number will be used in this chapter. We^* is the Weber number based on conditions at pinch-off, given by

$$We^* = \frac{\rho_d (u_j^*)^2 d_j^*}{\sigma} \qquad \textbf{(3.1)}$$

where u_j^* is the mean jet velocity at breakup, d_j^* is the jet diameter at breakup, ρ_d is the dispersed phase density and σ is the interfacial surface tension. The pinch-off conditions cannot wholly be controlled, but are dependant upon initial conditions of the flow and system. Figure 3.1 illustrates the features of the pinch-off region. Figure 3.2 shows the definitions for d_j^* and d_d^* which are used in calculating We^*. In order to make a comparison to the breakup length data of Meister and Scheele (1969a), the breakup length will be reported as a function of We, given by

$$We = \frac{\rho_d u_e^{\,2} d_j}{\sigma} \qquad \textbf{(3.2)}$$

where u_e is the mean jet velocity at the nozzle exit, d_j is the jet diameter at the nozzle exit. The parent droplet equilibrium diameters will also be reported against We due to the measurements being made downstream of the pinch-off location (which is explained in more detail in section 3.6). All other parameters of interest will be reported in terms of We*. The initial jet velocity profile is assumed to be parabolic at the nozzle exit (Gaspodinov et al, 1978) and it is further assumed that the velocity profile relaxes to a flat, step profile with appreciable shear between the jet and ambient interface.

In order to calculate We*, the jet velocity near pinch-off must be known. This was accomplished by using the nozzle exit flow rate and diameter of the jet across the last disturbance just before pinch-off. A circle exists that is bound by the jet whose area is calculated using d_j^*. Due to conservation of mass, the volumetric flow rate through this circle is equal to the flow rate exiting the nozzle. As long as the jet column is still intact, this methodology holds true. The velocity through an orifice equal to d_j^* is then simply calculated by dividing the volumetric flow rate at the exit by the area of d_j^* and this is taken as the jet velocity at breakup, u_j^*. Figure 3.3 shows the relationship between We and We*. The correlation shown is

$$\ln\left(\frac{d_j^{\,*}}{d_j}\right) = .318 \ln\left(\frac{We}{We^*}\right) + .098 \qquad \textbf{(3.3)}$$

with a correlation coefficient, R =0.998.

3.2 Flow Visualization

Figure 3.4 through Figure 3.7 show typical breakup sequences for the range of Re, We combinations studied. This series of figures demonstrates the topological transition that was observed in the pinch-off region as the exit velocity increased. For low values of We^*, the geometry in the pinch-off region is stable, that is little change is seen in the surface geometry before and after pinch-off. The droplets form at the tip of the jet at pinch-off in nearly the same location as all of the previous drops (see Figure 3.4). As the flow rate increases, We^* generally increases as well. The jet continues to break up with regularity with drops forming at the tip for $We^* = 0.31$, but the interface between the upstream jet and downstream drop becomes more elongated. The upstream and downstream cone angles are also observed to be more acute for $We^*=0.31$ than for $We^* = 1.9E\text{-}3$.

The present experimental uncertainties were dominated sampling limitations. The jet column length at breakup, upstream and downstream cone angles, satellite size and number, parent droplet size, ratio of separating droplet diameter to upstream jet diameter, and neck length were all studied and will be reported. As stated in section 3.1 above, Figure 3.1 shows the definitions of parameters of interest in the pinch-off region. The frequency of pinch-off events was recorded and found that the frequency generally increases with increased nozzle exit velocity. Figure 3.8 shows the general trend of increased frequency of occurrence with increasing We. There were generally only mild fluctuations in the frequency of the events, with the exception of the events recorded in the bi-modal region. As shown in the figure, these varied widely and the

variance is attributed to the switching of the mode back and forth between separating jet and separating droplet. There is a preferred breakup length for the separating jet and a different preferred location for the separating droplet in this region. We^* = 0.34 is shown in Figure 3.6. This test condition is near the transition region where the jet becomes bi-modal. The current image shows a double node being consumed to form a separating droplet at the end of the jet, which results in a large droplet. Figure 3.7 illustrates We^* = 2.12, which is past the transition from droplet separation to jet separation. This figure illustrates a pinching jet where a droplet will separate from the tip of the intact jet shortly thereafter. Multiple nodes near a pinch-off event were often observed in the pinching jet region.

3.3 Breakup Length

The breakup length of the liquid jet is one of the most widely studied details of jet disintegration. Although there is a lot of data on breakup length, which in turn has been used to develop theoretical correlations and numerical models, there are still discrepancies in how the breakup length is measured. There are generally three different ways to consider the breakup length; 1) the distance from the nozzle exit to the first separation [Lin, 2003] which shall be termed l_b hereinafter, 2) the distance from the nozzle exit to the location of the jet farthest downstream that is still intact at the moment of breakup (present), termed l_a hereinafter, or 3) the location measured from nozzle exit at which the most regular disturbance breaks the jet [Grant and Middleman, 1966]. Grant and Middleman (1966) argue that the location of first separation is unreasonable due to the erratic behavior of this location for some test conditions,

however using their method of where the most regular disturbance breaks ignores the fact that the jet does break at different locations in a fairly regular manner for these test conditions.

The breakup length may be manipulated by imposing an artificial disturbance on the jet, which forces the breakup to occur at a specific location which is closely tied to the frequency of the artificial disturbance [Webster and Longmire, 2001]. The present study uses the second definition, the total column length at breakup. This definition takes into account Grant and Middleman's (1966) argument that the point of pinch off is erratic as the total column length is much more stable than the pinch-off location in the transition and Weber regimes. No artificial disturbances were intentionally introduced into the system for this study. Figure 3.9 illustrates the two definitions l_a and l_b. Although the correct description of the breakup length at breakup is the total column length, both the total column length and length to breakup data are reported in Figure 3.10.

The breakup length of the expanding jet, as shown in Figure 3.10, was found to follow the same trends as other experimental data [Meister and Scheele, 1969a and Tyler, 1932]. Furthermore, a similar map has been published for the generalized breakup of liquid jets [Lin, 2003] which shows agreement with the data taken in this experiment. This general trend is also consistent with published results of Grant and Middleman (1966) for liquid in air jet breakup.

The typical breakup regimes for liquid-liquid systems are Rayleigh breakup (also known as varicose), Weber breakup (also known as sinuous) and atomization. Based on the large FOV images taken for the column break up length study and the historical definition of transition, the transition from Rayleigh to Weber is seen to occur near We = 1000 (We^* = 2.121). As was the case in the literature [Meister and Scheele, 1969a], the breakup length grows to a maximum and then begins to shorten with increasing nozzle exit velocity. Figure 3.10 shows the Rayleigh breakup regime for the current experiment, which is considered to be the region where the jet length increases with increasing velocity (We number) as well as the Weber or sinuous breakup regime, which is considered to be the region where jet length decreases with increasing velocity [McCarthy and Molloy, 1973].

The stability of the breakup location was found to be strongly tied to the breakup regimes. When the breakup mode was solidly within the regime (Rayleigh or Weber), the variance was small. When the mode was mixed, there was a wide variance in the breakup location. This is clearly illustrated in Figure 3.10. The maximum in the breakup length curve is widely attributed to the viscous effects of the ambient fluid. The transition between drop-pinching and jet-pinching (as shown in the inset of Figure 3.10) is not well understood, however. In the transition region, the jet breakup location is closer to the nozzle exit whenever the jet pinches off into a second jet and further from the nozzle exit when the jet separates into a droplet.

No one has previously reported on the length of the column between the pinch-off location and the farthest downstream location that is still intact at pinch-off. This is believed to be the first time a study has been reported on this particular characteristic. Figure 3.10 shows that the difference between l_a and l_b increases at first (which is attributed to the changeover from a separating droplet to the separation of multiple intact nodes) and that the maximum difference in these two locations is in the region of transition from droplet pinch-off to jet pinch-off. Just as the overall breakup length reaches a maximum, so does the difference between l_a and l_b. As the exit velocity is increased further past the point of maximum jet length, the difference begins to become less noticeable. This is attributed to the fact that the jet is observed to pinch-off in multiple locations within the transition regime (termed bi-modal) and then the pinch-off location stabilizes after the velocity is increased further into the pinching jet regime.

3.4 Pinch-Off Angles

The upstream and downstream cone angles were also studied in an effort to determine where the crossover point between the various breakup modes lies. No delineating information was found to distinguish between primary droplet breakup and primary droplet breakup with satellites (one or multiple), however the difference in droplet breakup and jet breakup was observed to be the point at which the upstream angle becomes equal to or larger than the downstream angle (i.e. the downstream angle becomes more acute).

Figure 3.11 shows the upstream and downstream cone angles as a function of the Weber number at breakup, We^*. The upstream angle is more stable than the downstream angle, as shown by a smaller change between lower and higher values of We^*. The correlation for the downstream cone angle is given by

$$\theta_d = -38.935We^* + 140.92 \quad \textbf{(3.4)}$$

with a correlation coefficient of *R=0.904.* The correlation for the upstream cone angle is given by

$$\theta_u = 15.823We^* + 75.24 \quad \textbf{(3.5)}$$

with a correlation coefficient of *R=0.695.* At We^* =11.5, the downstream angle becomes equal to the upstream angle and the mode of breakup changes from mostly droplet separation to jet or column separation. The separating jet is shown in Figure 3.12.

This data suggests that the crossover between jet-pinching and drop-pinching occurs when the upstream and downstream cone angles are equal. The experiments showed only droplet pinch-off for low values of We* with a mixed mode (also referred to as bi-modal) for moderate values of We^* and purely jet pinch-off breakup for the highest values of We^* studied. In the region of transition, droplet separation occurs more often than the pinching jet at first and slowly moves toward the pinching jet dominating the pinching droplet. The breakup map for Rayleigh to Weber breakup is presented in Figure 3.13. The transition zone that was observed in this study is labeled bi-modal because both varicose and sinuous breakup modes were observed at these test conditions with regularity. The map shown in Figure 3.13 corresponds to the portion of Figure 3.10

up to We = 1200. During the study for breakup length, some flow irregularities were observed at lower We that appeared similar to the disturbances commonly observed in the sinuous breakup regime. These disturbances usually appeared about one-third of the way from the nozzle to the end of the jet and often would equalize to a large varicose type disturbance upstream of the location that would be expected to pinch-off (see Figure 3.14).

3.5 Droplet to Jet Diameter Ratios

The droplet to jet diameter ratio was also studied in detail. Skelland (1974) reported that Rayleigh (1892, 1899) first deduced an approximation for the size of a droplet separating from a liquid jet. This value is widely known to be

$$d_d = 1.89 d_j \tag{3.6}$$

for a liquid jet in air. However, Christianson and Hixon (1957) confirmed a similar value for liquid-liquid systems of 2.01 while Tyler (1933) reported a value of 1.91 for liquid-liquid systems. Skelland (1974) suggests that the diameter of the jet should be taken at breakup, which corresponds to d_j^* in the present study. Figure 3.15 confirms this value for the Rayleigh breakup regime, however a linear reduction in droplet diameter is seen after the transition from droplet to jet breakup.

The lower plot of Figure 3.11 shows the primary droplet to jet diameter ratio at breakup across the Rayleigh and into the Weber regimes. The droplet to jet diameter ratio matches the Rayleigh limiting value of 1.89 well in this region, with values larger than this attributed to the number of nodes that were consumed during drop formation [Das,

1997]. Figure 3.16 shows the data of the current study plotted along with that of Das (1997) for the present viscosity ratio of 0.152. Das argues that the number of nodes and the diameter of the jet at pinch-off govern the final size of the separating droplet. The data of the present study supports the conclusions of Das (1997) up to the point of transition from droplet pinch-off to jet pinch-off. The correlation proposed in the present study for the final droplet size in the transition region from droplet pinch-off to jet pinch-off (and up to atomization) is

$$\frac{d_d}{d_j} = -.00878We + 21.44 \qquad \textbf{(3.7)}$$

with a correlation coefficient of *R=0.953.*

In addition to the cone angles becoming equal at the transition point, the diameter across the first maxima downstream of the pinch-off location became equal to the diameter across the last disturbance before the pinch-off location. This explains why the cone angles become the same at the transition. Figure 3.13 also shows that the point at which the upstream and downstream diameters are equal ($d_d^*/d_j^* = 1$) corresponds to the same point at which the upstream and downstream cone angles are equal.

3.6 Primary Droplets

At low We, the liquid jet can be observed to actually flow into the drop forming at the end. The drop is observed to fill like a balloon and eventually stretch and pinch-off from the main jet. As We increases, the separating drops do not grow as large before they separate. The primary droplets are observed to decrease in diameter with

increasing We, as also reported by other researchers. However, in the present study, the primary droplets never became smaller than the initial jet diameter which conflicts with results of other researchers [Liu, 2000] which is attributed to the expanding jet. If the average jet diameter just before pinch-off is assumed to be equivalent to a non-expanding jet issuing from the nozzle exit, the resulting droplet diameters would agree with Liu (2000) which was the approach used by Skelland (1975).

The data is taken far downstream from the pinch-off location after the drops are observed to have reached an equilibrium shape. This figure is presented against the We number referenced to the nozzle exit rather than at breakup because the droplets far downstream could not be correlated to the pinch-off event that created them, and therefore pinch-off conditions (v_j^* and d_j^*) could not be used with any accuracy.

The diameter of the separating droplet (or jet) at pinch-off is shown in Figure 3.17. It is plotted along with the jet diameter. Each result has been normalized by the jet diameter at pinch-off. What is significant is that in the region of transition, the primary droplet diameter varies significantly from the rest of the data points and does not fit the general trend. The data from these two parameters intersect at the same test condition (approximately $We^* = 11.5$ or $We = 600$) as previously presented, which further supports the claim that the changeover occurs when the cone angles and upstream and downstream angles are equal.

The final key observation to report is on the uniformity of the parent droplets. The parent droplets were seen to have very uniform diameters in the Rayleigh regime. The parent droplet diameter began to vary as the transition point was approached and varied the greatest after transition. Figure 3.18 shows the variation in size distribution with increasing nozzle exit velocity. Figure 3.18 (a) shows the uniform droplets in the Rayleigh regime, (b) shows the bi-modal transitional regime and (c) shows the Weber regime.

3.7 Satellite Droplets

Due to the lack of a good definition for satellite droplets and the fact that some researchers [Tjahadi et al., 1992] consider a satellite droplet to be smaller drops between large primary droplets, a clear definition of a satellite droplet is needed. For the purposes of this study, a satellite droplet is defined only as a droplet (or droplets) that form from the fluid in the neck region of a pinch-off event. In most cases, the satellite droplet is therefore much smaller in diameter than the primary (or parent) droplet, but it also leads to situations where satellite droplets are nearly the same size as the parent droplet.

Satellites were observed in every experiment. The number of satellites varied but no correlation was seen between number of satellites and We^* or frequency of satellite formation and We^*. The frequency of satellite formation in this instance is simply the percentage of breakup events in which a satellite was observed to have formed. The first and second satellite droplets were measured to be nearly the same size at the

transition from Rayleigh to Weber, but no other definitive relationship was seen so this may be purely coincidental. However, the size of the satellite droplets did show a dependence on We. The size of the first satellite droplet approaches a maximum at the transition point (based on the present results of transition occurring when upstream and downstream cone angles are equal) and the frequency of the second satellite approaches a minimum at this point.

The second satellite droplet appears to follow almost a parabolic growth profile. This is illustrated in Figure 3.19 where the frequency of the second satellite is shown to increase immediately after the transition point. No more than two satellites were observed for a separating droplet, but up to three satellites were seen in the jet-pinching regime. The number of pinching events observed in the present study that resulted in more than two satellite droplets was not sufficient to report statistically meaningful information about their behavior

3.8 Neck Length

The neck length measurement should be considered the least accurate of all the measurements taken and will be the most difficult for other researchers to duplicate. The best definition of the neck length merely suggests that it is the region that stretches out during a pinch-off event. Since the actual beginning and end of this region is not clearly visible, the researcher must make his own determination as to where the neck begins and ends. For the purposes of this study, the neck was taken to be the region

between inflection points on the upstream and downstream sides of separation (as shown in Figure 3.1).

The neck length between the upstream and separating segments was observed to lengthen with increasing We^*, although there appears to be a maximum in the data that suggests the profile may be more parabolic in this region than linear. The We number where this maximum occurred did not, however, correspond to the same test condition as the maximum column length or to when the upstream and downstream cone angles are equal when normalized by d_j but when normalized by d_j^* the maximum corresponded to exactly the same test condition as the cone angles being equal (as shown in Figure 3.20), which further supports the idea of the pinch-off event being localized in both space and time.

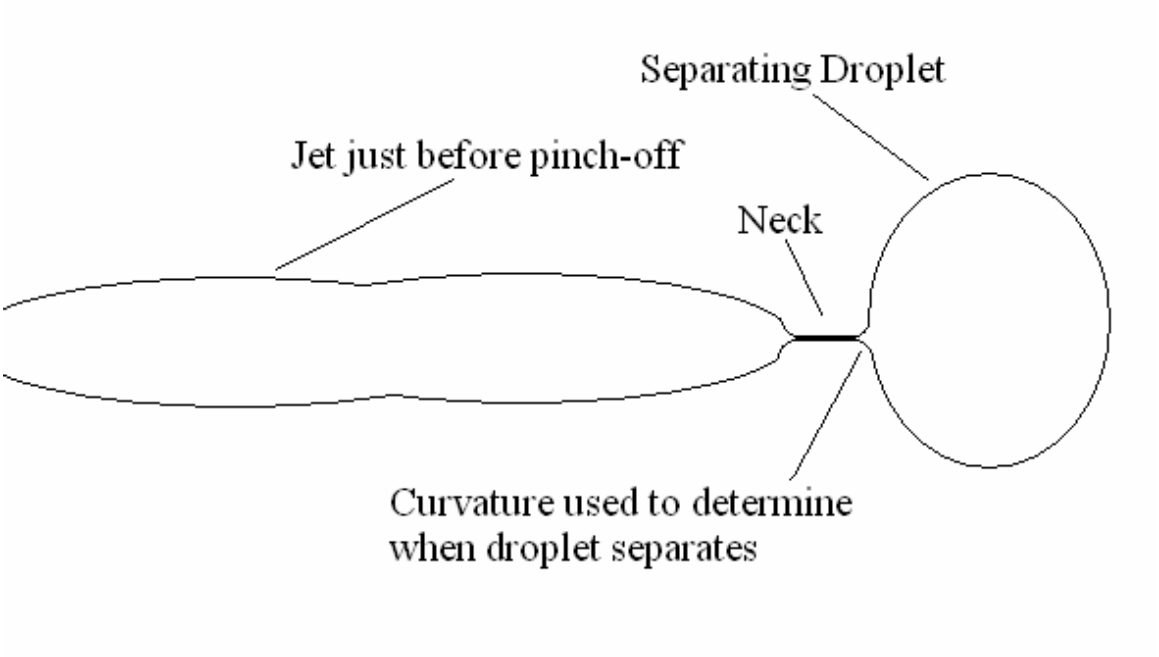

Figure 3.1 Schematic of pinch-off condition definitions

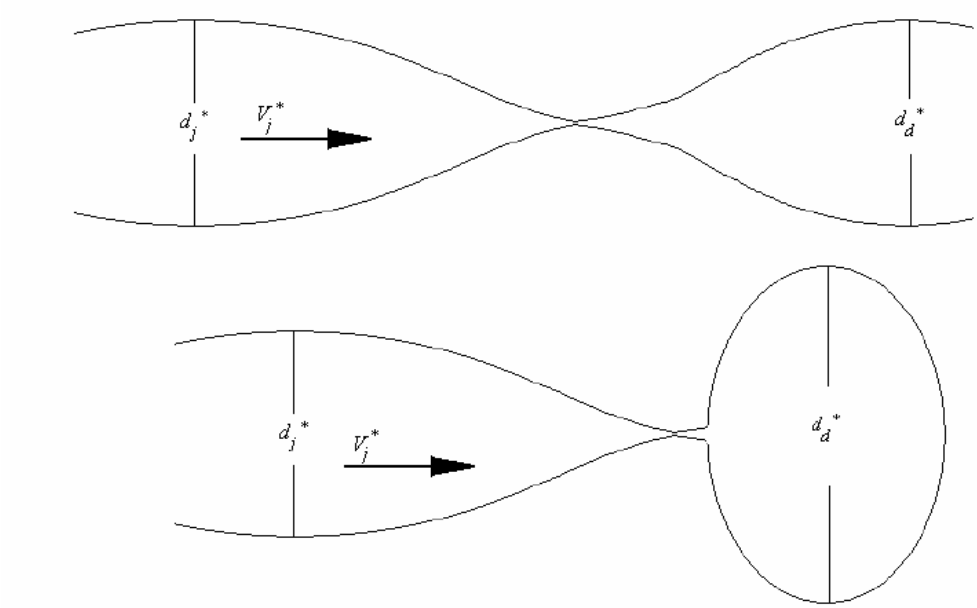

Figure 3.2 Definition of separating droplet, d_d^* is taken as diameter across first maxima after pinch-off.

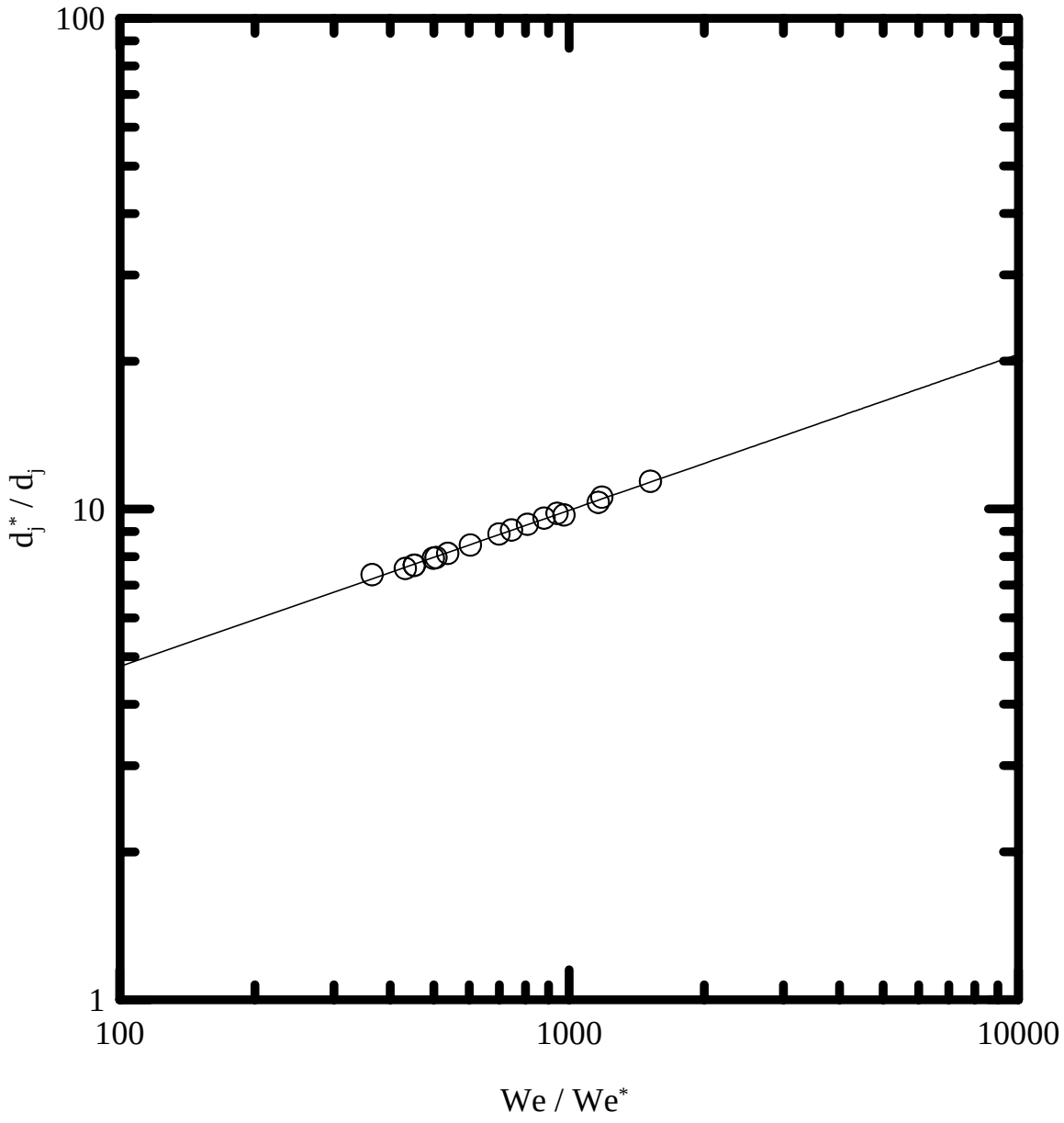

Figure 3.3 Correlation of We and We*

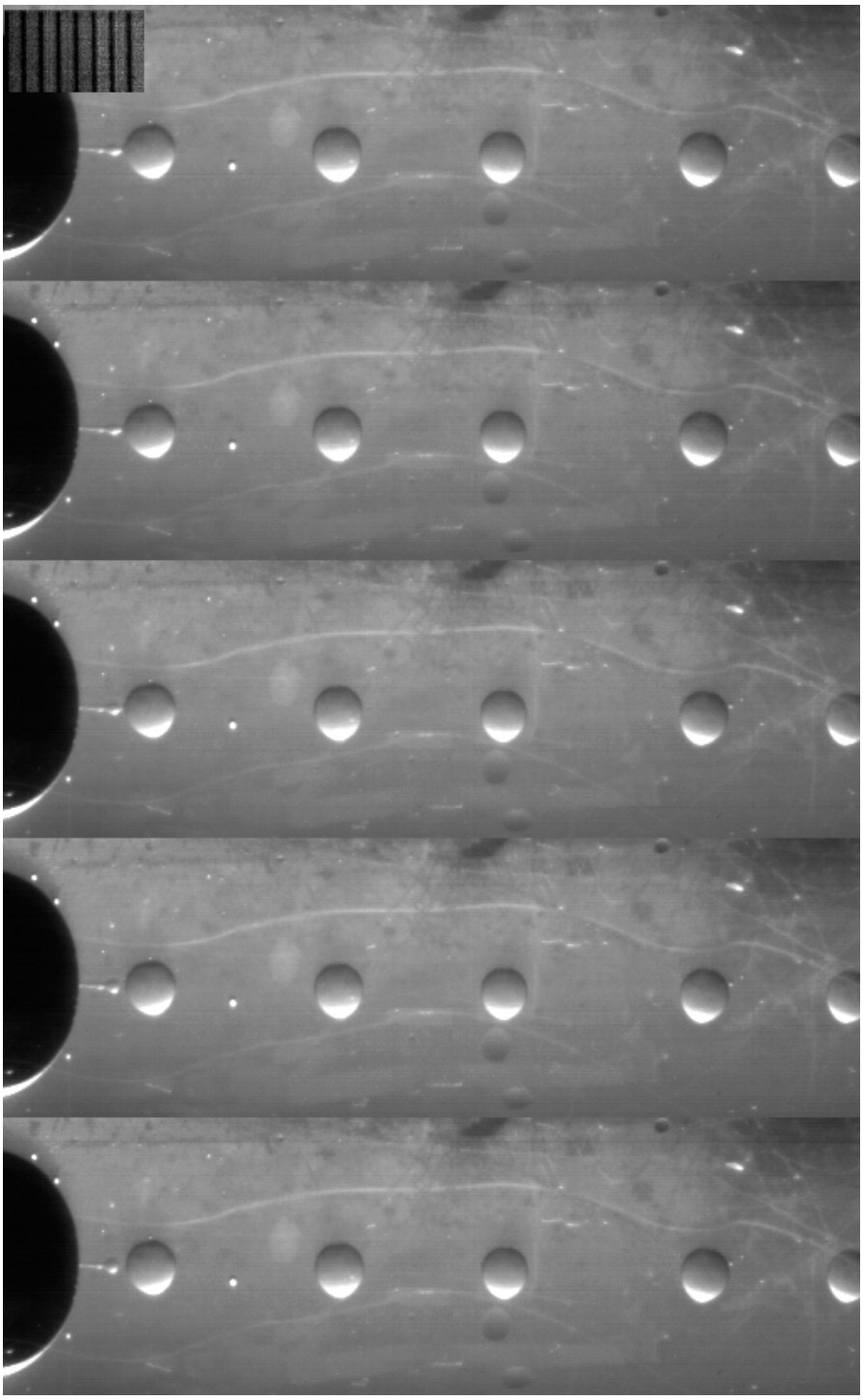

Figure 3.4 Re = 27, We = 11, We^* = 1.9E-3 droplet separation. Images separated by 5 frames, initially taken at 7500 fps (shown separated by 66.67 μs). Scale markings correspond to 1 mm.

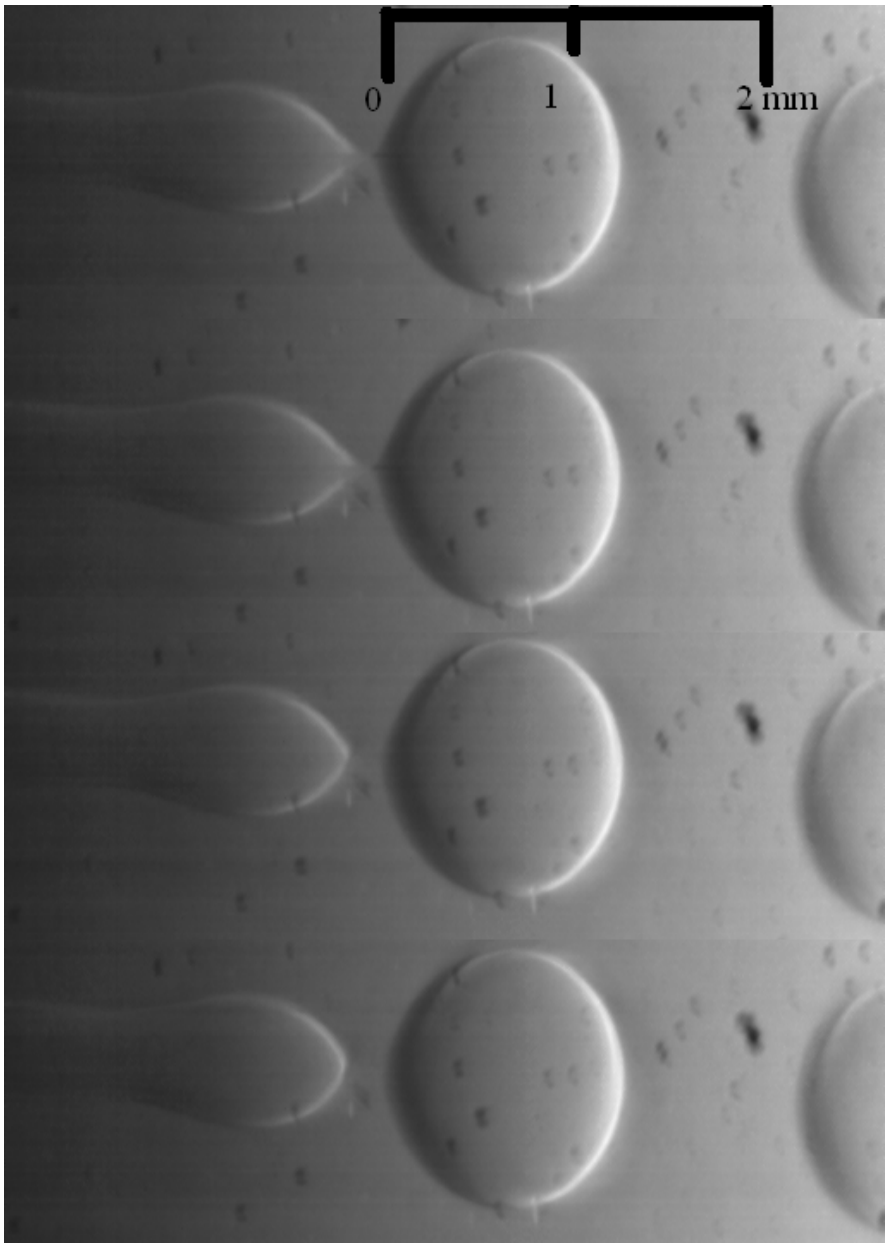

Figure 3.5 Re = 90, We = 134, We^* = 0.31 standard breakup sequence taken at 8830 fps (11.33 μs apart) , shown sequentially.

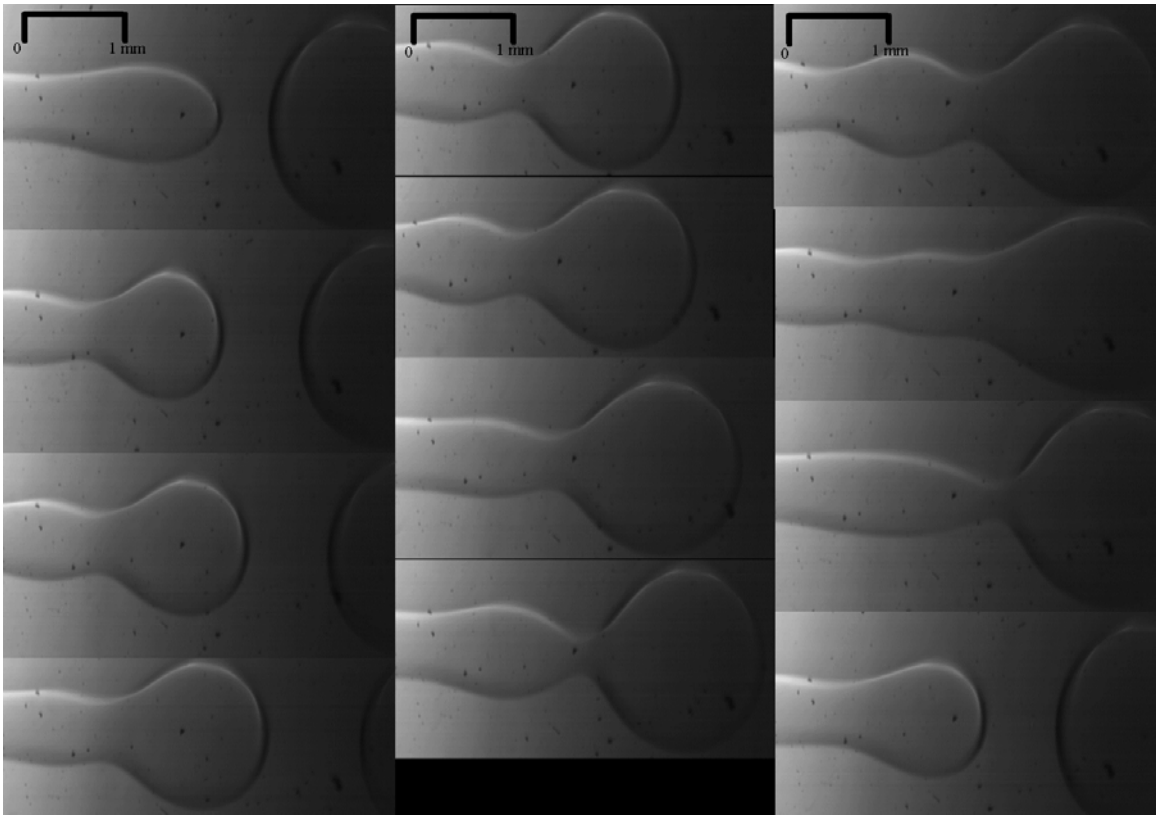

Figure 3.6 Re = 123, We = 260, We^* = 0.34 single mode observed. Photos taken at 16,000 fps (6.25 μs apart). Each image separated by 24 frames. One entire breakup sequence is shown.

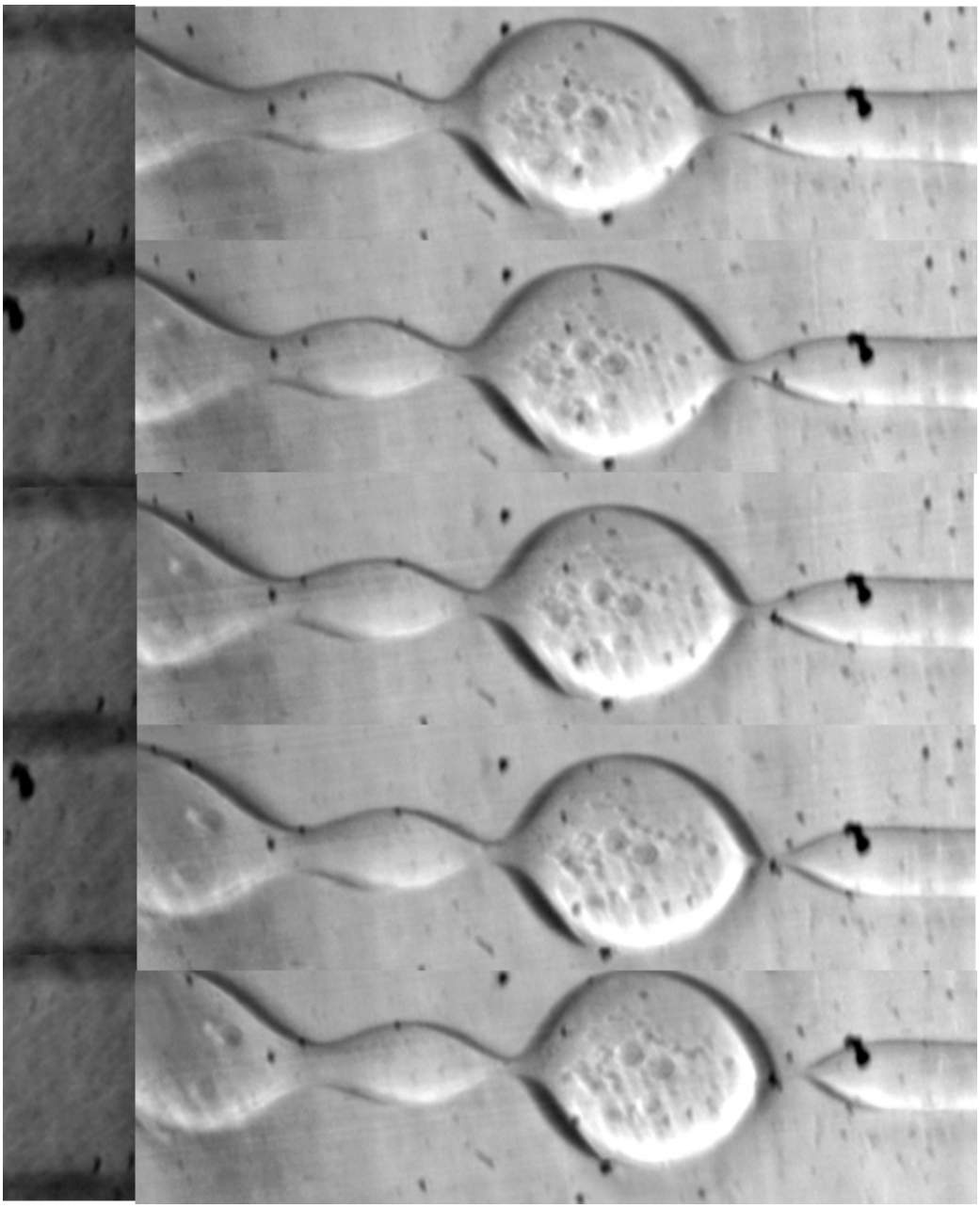

Figure 3.7 Re = 241, We = 961, We^* = 2.12. Images shown sequentially, taken at 8600 fps (shown 11.63 μs apart). Scale image shown at left corresponds to 1 mm markings.

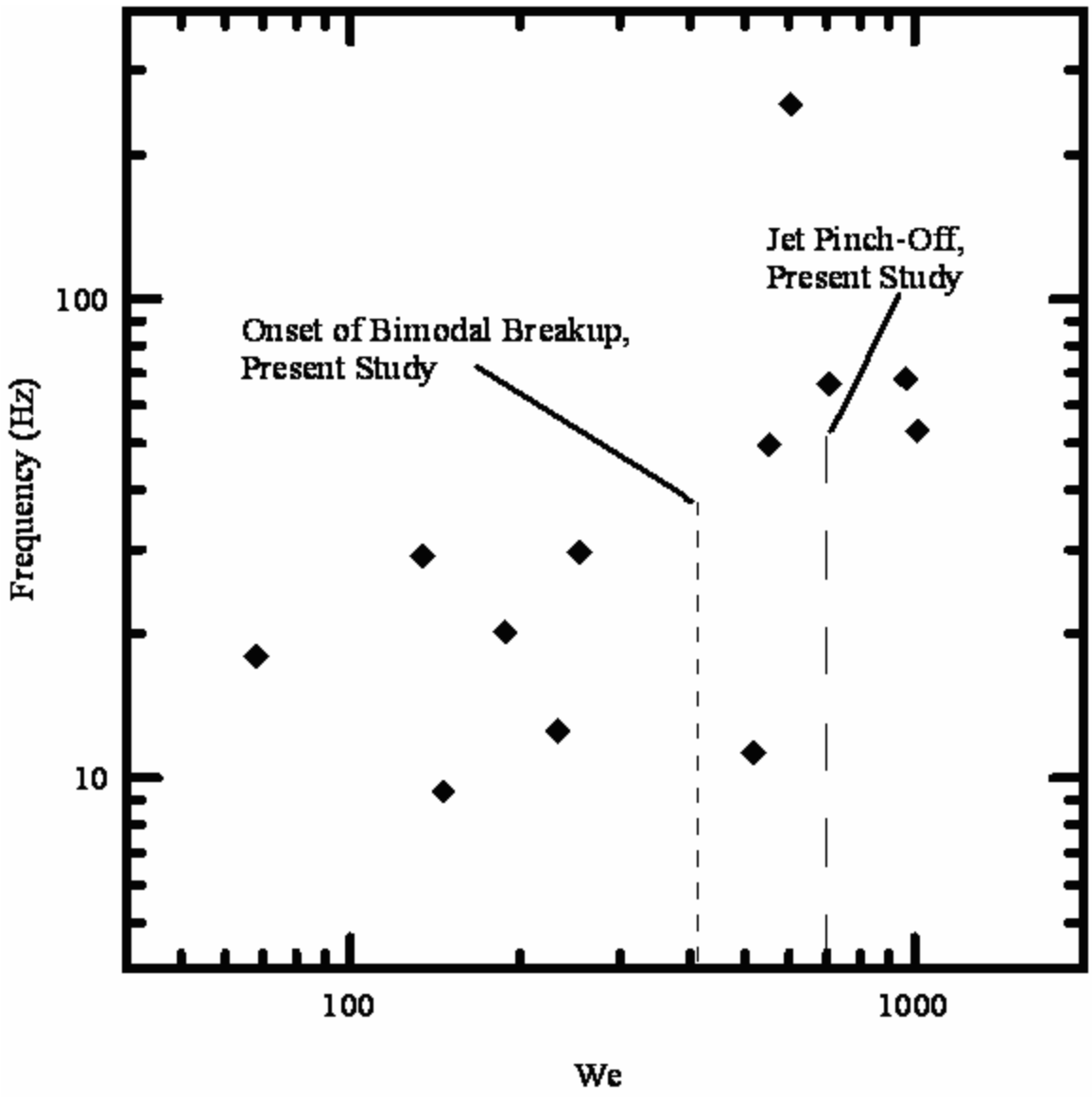

Figure 3.8 Frequency of pinch-off events

Figure 3.9 Definition of l_a and l_b

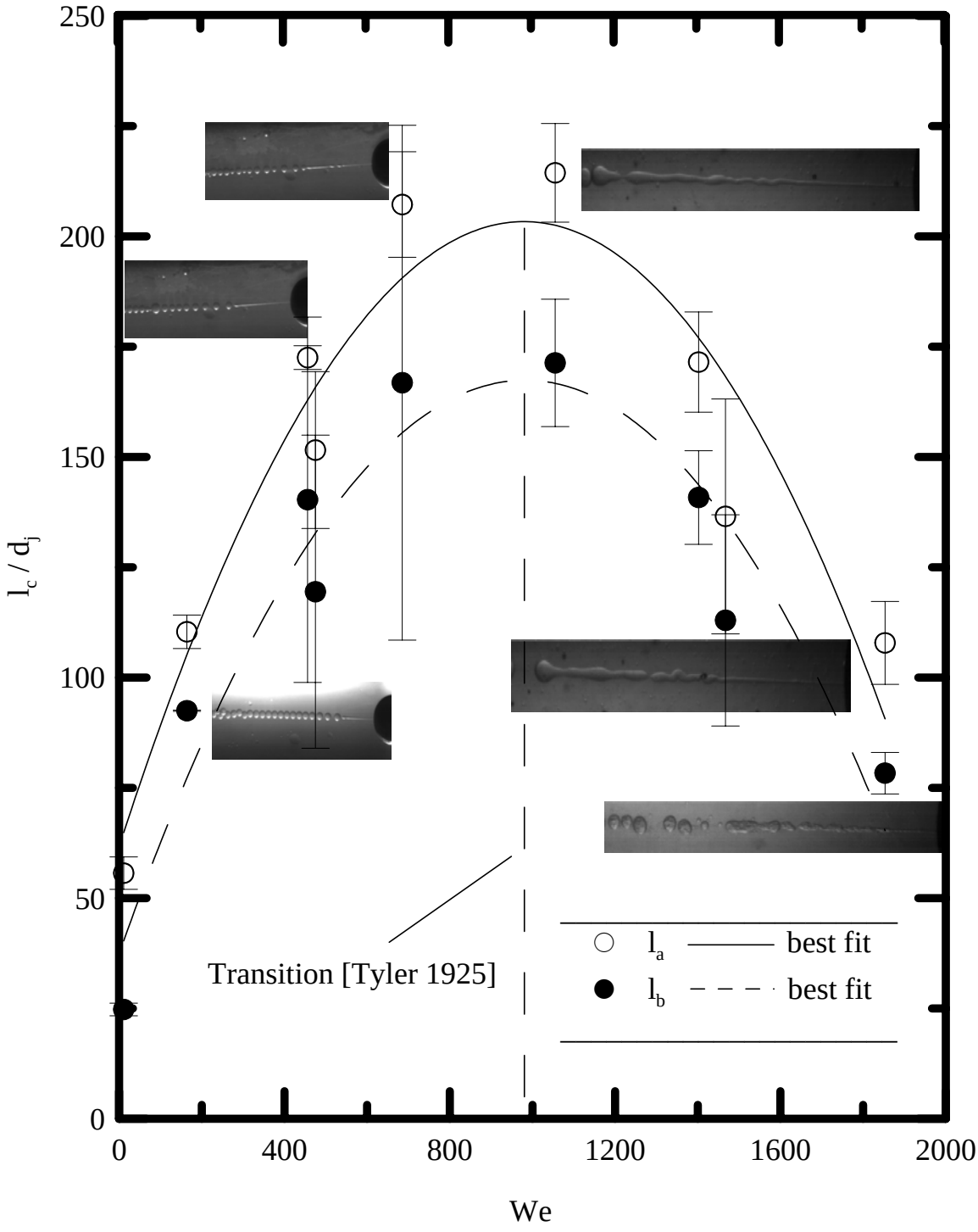

Figure 3.10 Dimensionless breakup length as a function of We, present experimental data. Inset images are adjacent to the test condition at which they were taken. Large FOV images on left side of graph show 48 mm FOV, small FOV images on right side of graph correspond to 18mm FOV.

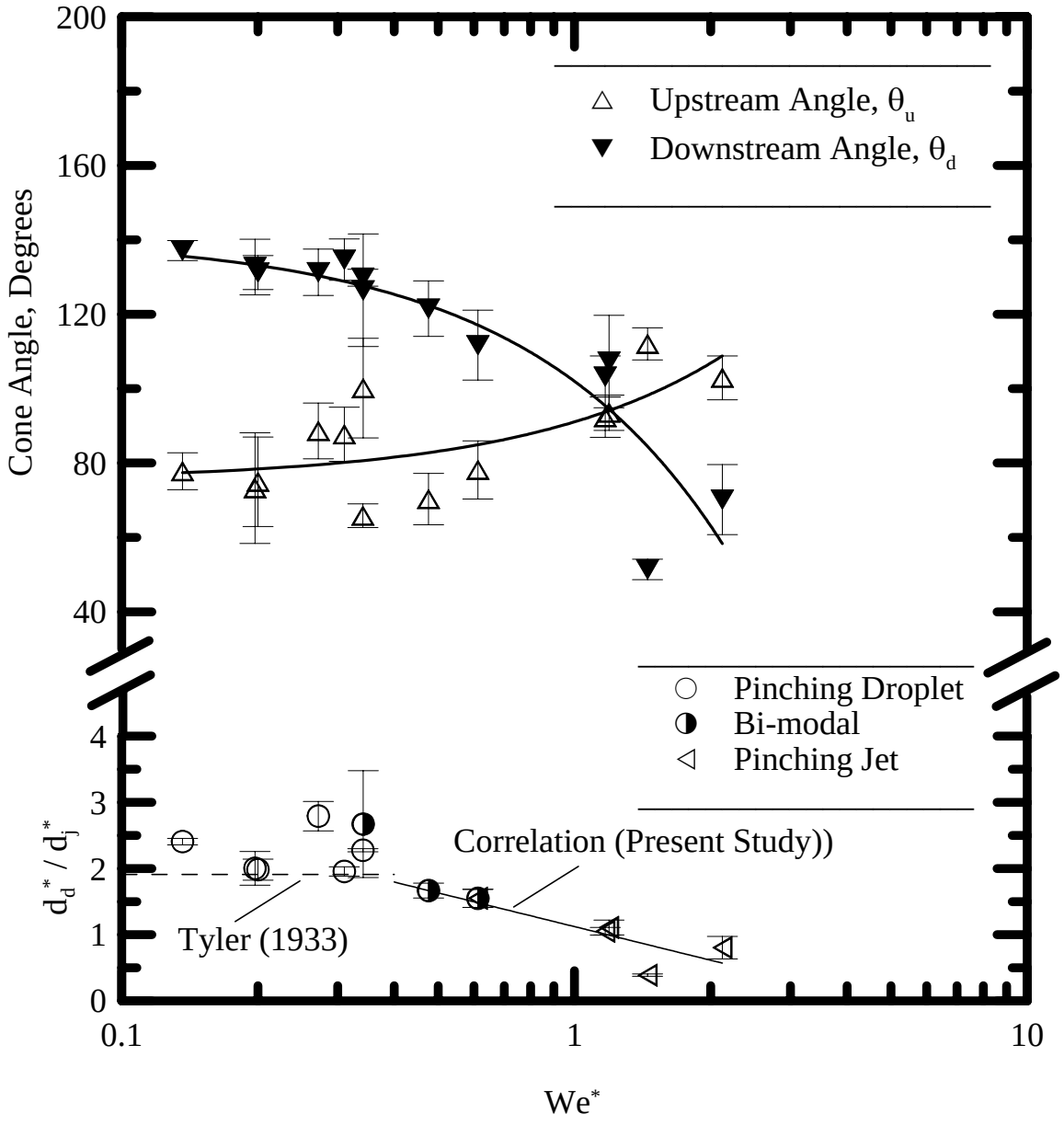

Figure 3.11 Separation angles shown for both upstream and downstream separation. Correlation equation d_d^*/d_j^* = -0.7341135303 * ln(We^*) + 1.122317939 Correlation Coefficient = 0.777.

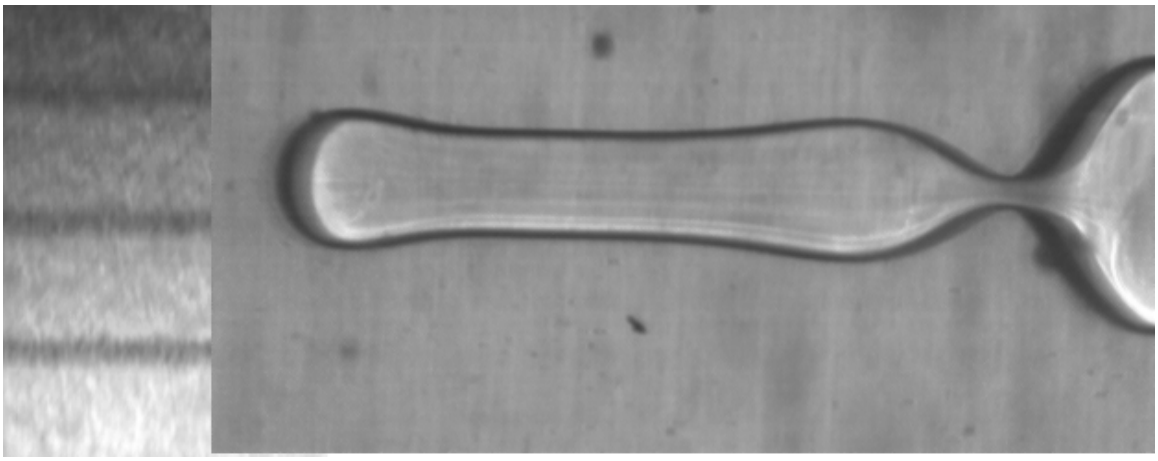

Figure 3.12 Re = 177, We = 500 Separating Jet. Calibration image shown at left, 1 mm increments shown.

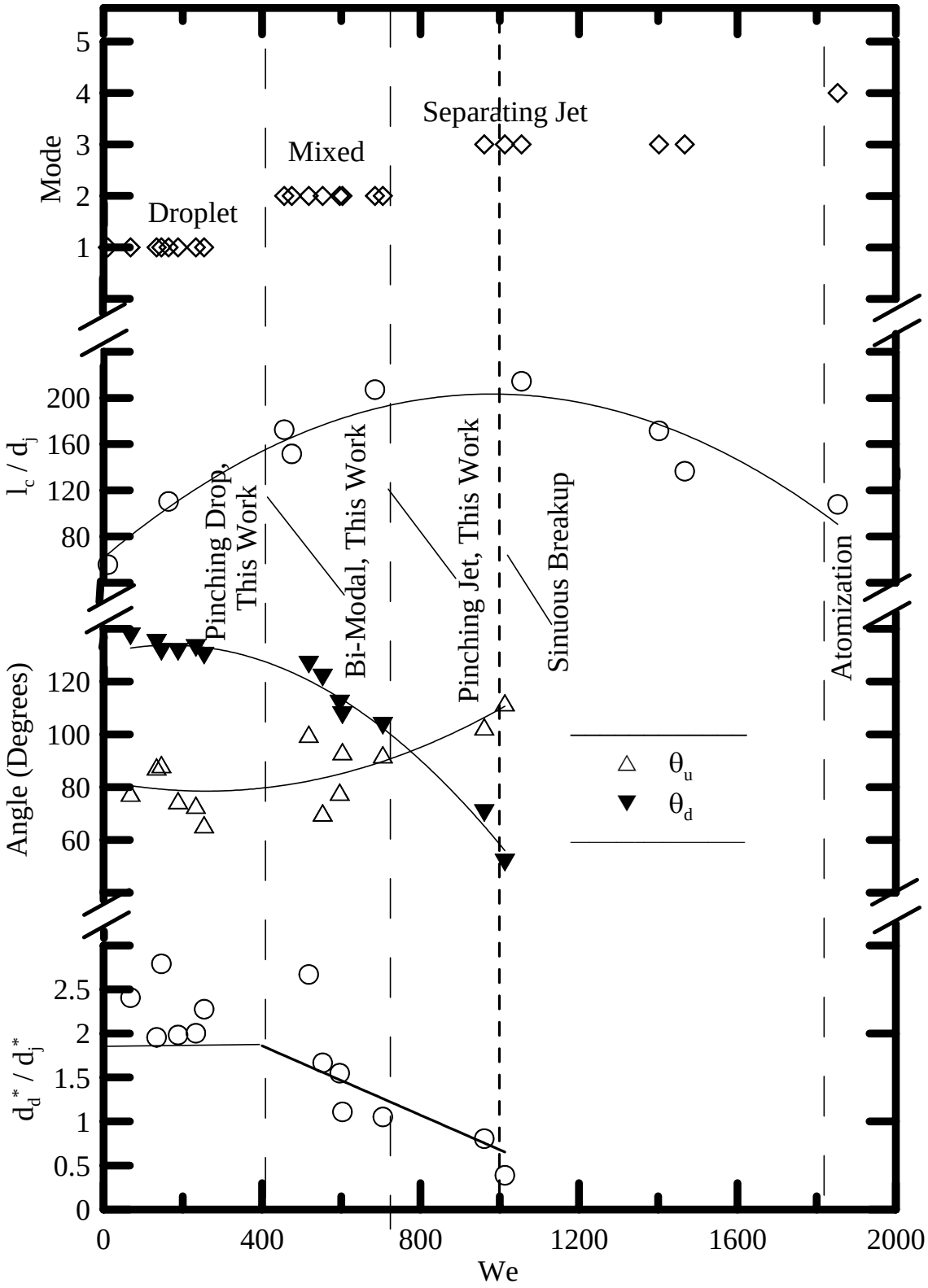

Figure 3.13 Breakup map showing boundaries of bi-modal (transitional) and Weber breakup regimes.

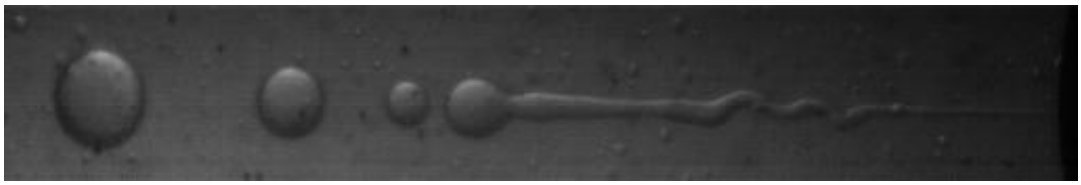

Figure 3.14 Flow irregularity resembling sinuous breakup mode of jet disintegration. We = 475, We^{*} = 0.0115.

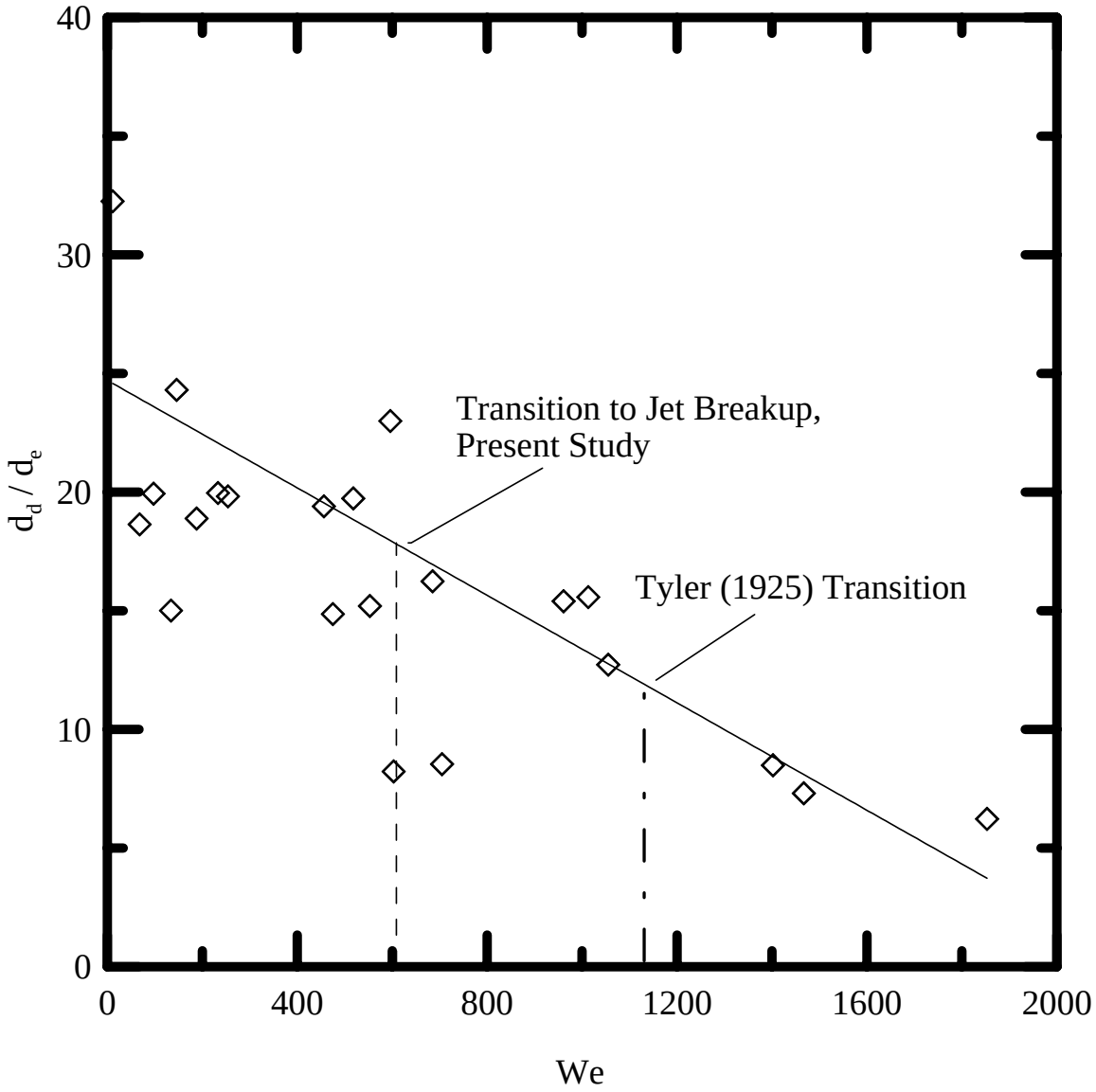

Figure 3.15 Diameter of parent droplets as a function of increased We number. Taken from large FOV images.

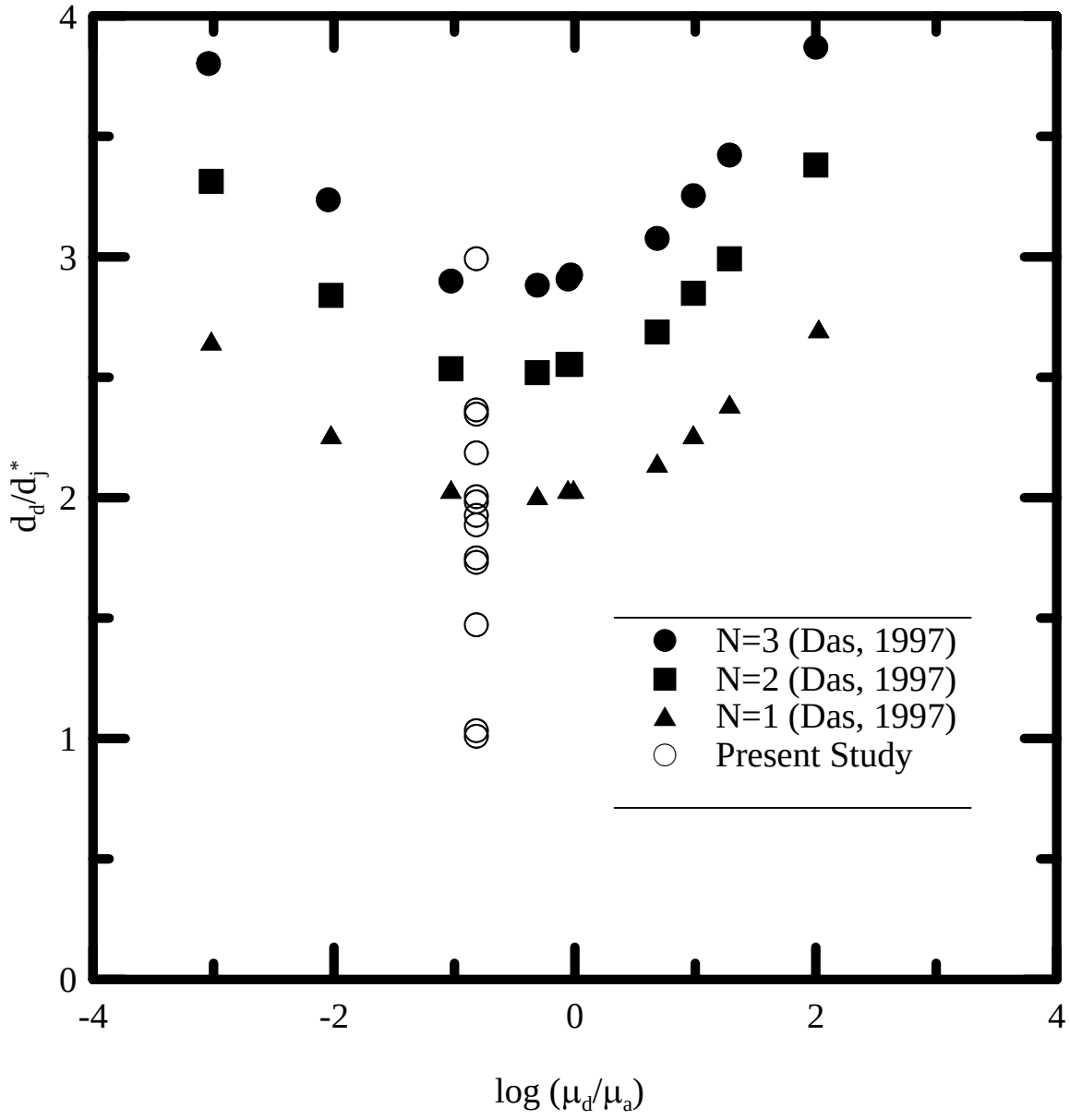

Figure 3.16 Final droplet size to jet diameter at breakup ratio analysis of Das (1997)

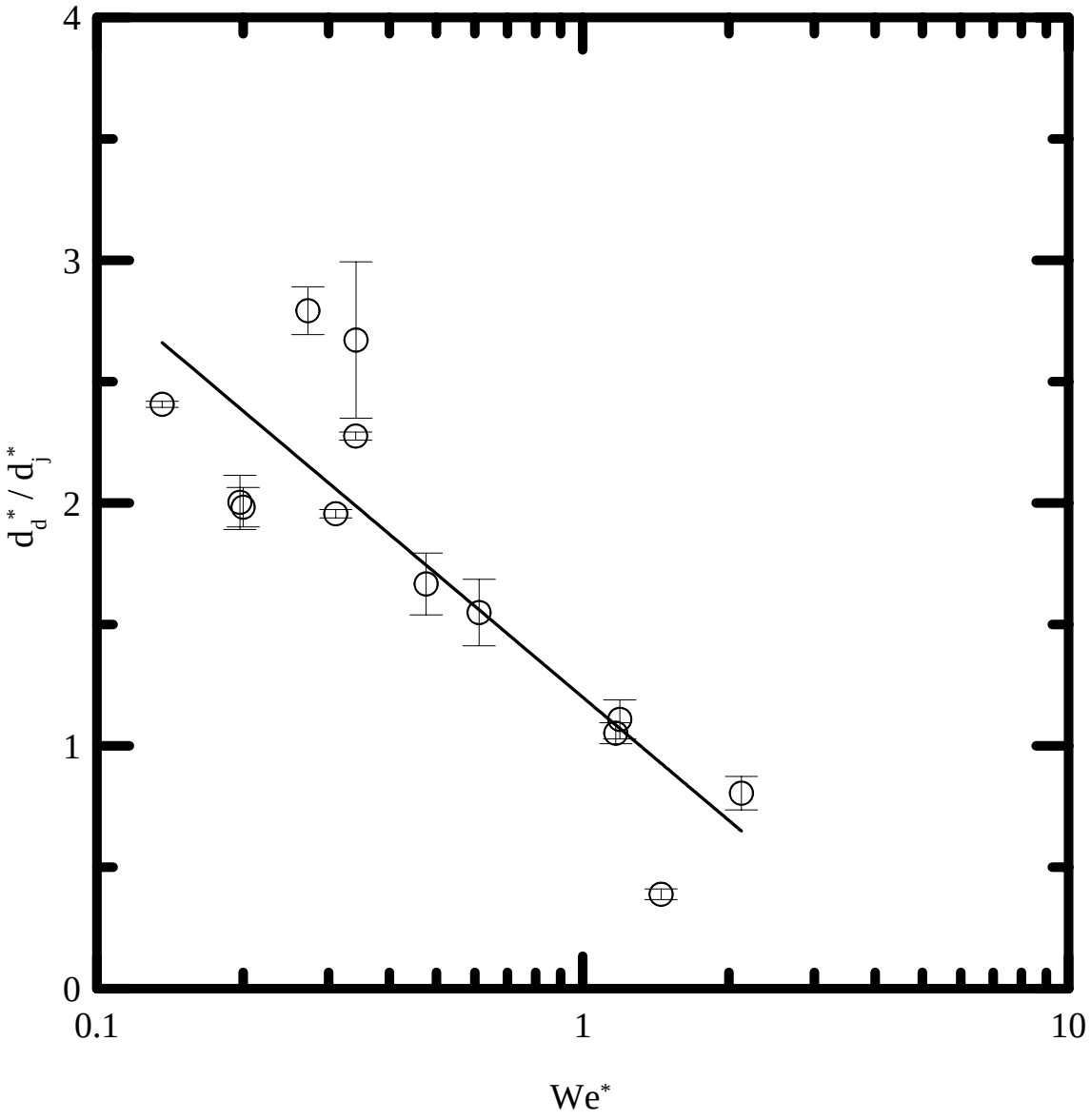

Figure 3.17 Dimensionless jet and drop diameters at pinch-off vs. We^*

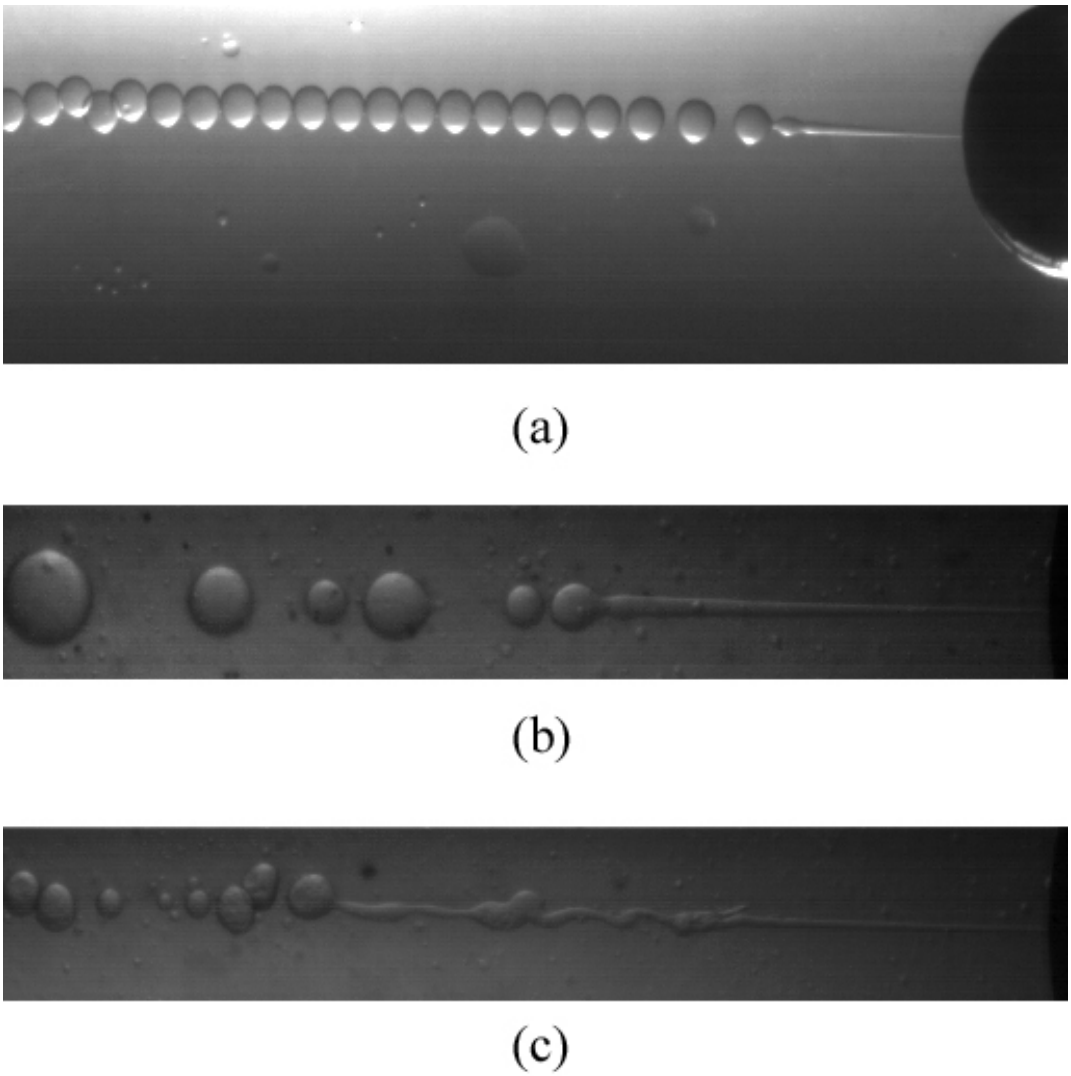

Figure 3.18 Droplet size distributions for (a) Re =50, We =41 (b) Re = 165, We = 456 (c) Re = 297, We = 1467. Jet diameter at exit = 100μm in each image.

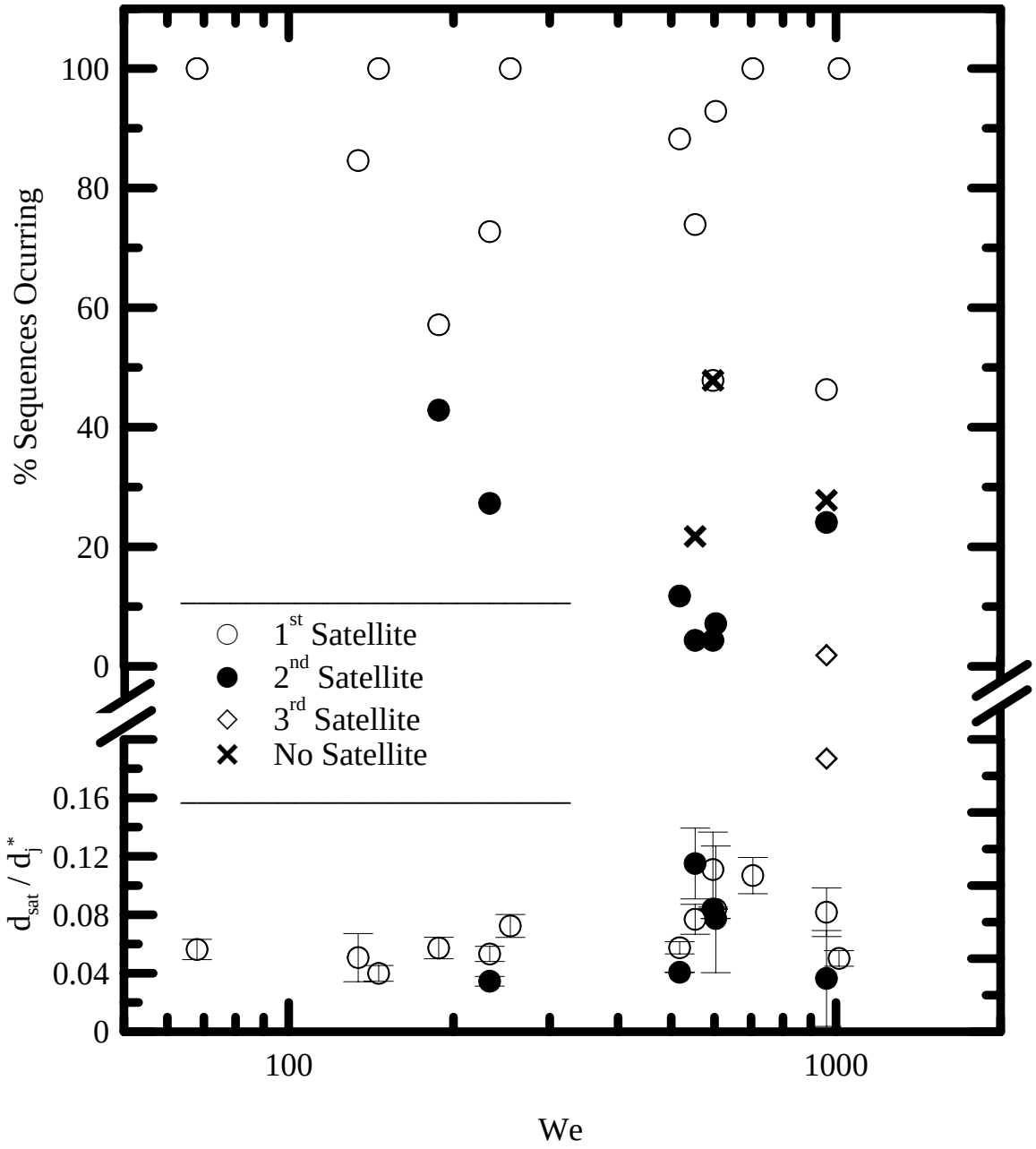

Figure 3.19 Frequency of satellite formation and normalized satellite diameters.

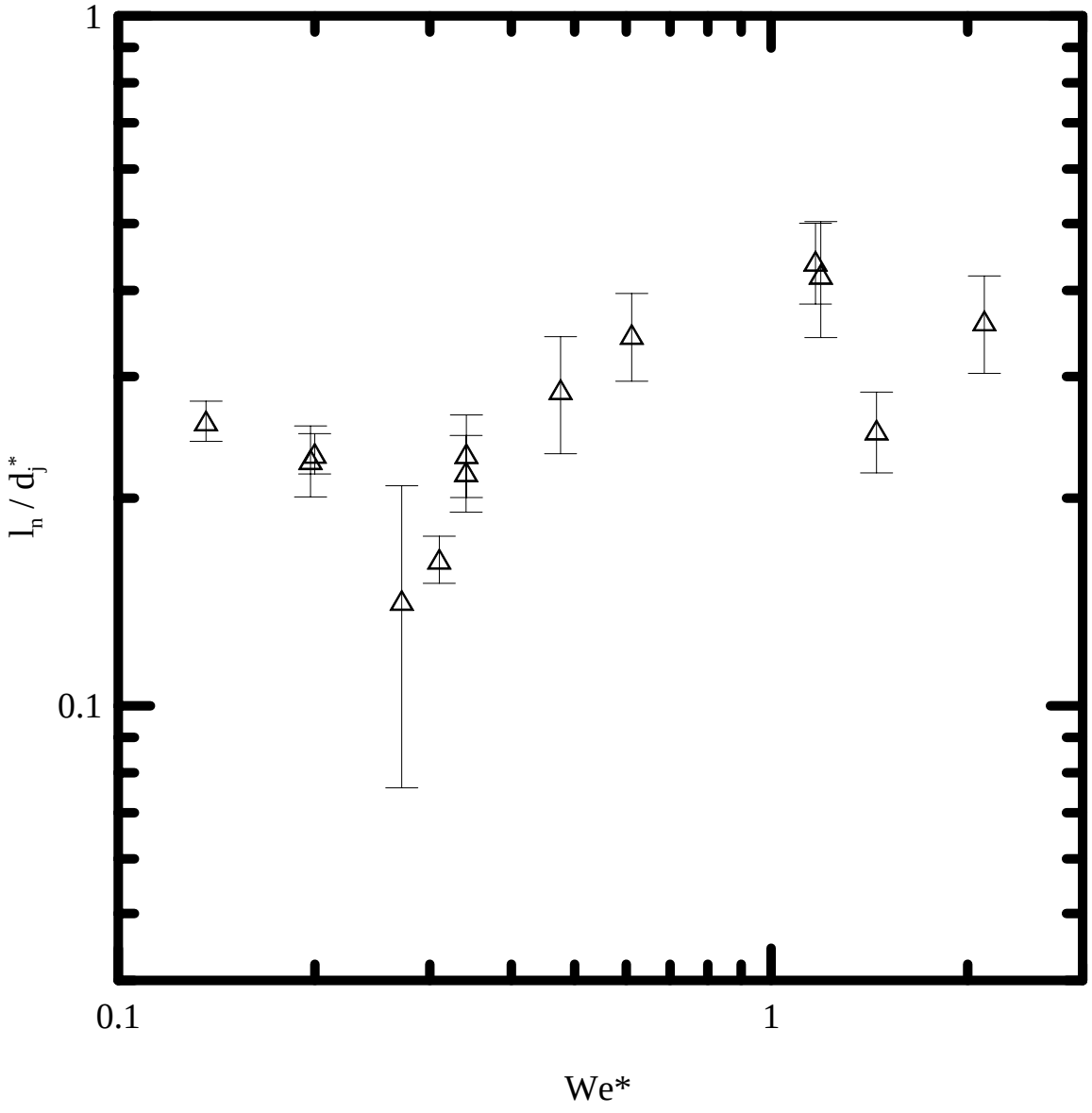

Figure 3.20 Neck length at pinch-off

Chapter 4

Conclusions and Recommendations

4.1 Summary

Classical experiments have generally shown a constant diameter or contracting jet, which allow broad assumptions to hold quite well. However, as was first reported by Das (1997) and verified in the present study, the jet may actually expand. In the case of the expanding jet, traditional equations and theories based on exit conditions and nozzle diameter cannot be applied without modification.

The present study considered a single liquid-liquid system with a single nozzle. The dispersed phase used was a mixture of distilled water and glycerin (53.4% water by weight) which was injected through a 97 μm nozzle into an ambient of Clearco 50 cSt 99.9% pure silicone fluid (DiMethyl PoliSiloxane). The exit velocity was varied from 1.7 to 16.3 m/s. Only the region up to and including transition to sinuous breakup has been considered. A parametric study to determine the full applicability of the forthcoming conclusions should be undertaken.

4.2 Conclusions

This study has shown that an expanding liquid jet flowing in a second immiscible liquid has similar behavior to previously studied configurations in only a limited number of ways. The micro liquid jet expanded to the macro scale before disruption in every case

that was studied. It is still not clear if the primary driver for this is nozzle geometry, a competing balance between drag and inertial and surface tension forces, or a preference for a particular capillary diameter and geometry for the breakup to occur. For the test conditions studied, the major conclusions are:

1. The dependence of breakup mode upon the separation diameter to jet diameter ratio at pinch-off is significant and has been reported. Previous works have concentrated on the diameter of the separated droplet to the initial jet diameter, however in the case of an expanding jet the classical theories on what this ratio should be do not hold. The initial conditions at the nozzle exit do not govern the pinch-off event. While only the exit velocity was changed in the present study, the change in the jet diameter between the nozzle exit and breakup location dictates that the jet is not well described by the exit conditions by the time it reaches the point of breakup. The present work has shown that the flow characteristics and geometry of the jet in the region of pinch-off control the jet breakup. The present study supports the conclusions of Das (1997) which suggest that the size of the droplets separating from the jet is dependant upon the conditions at pinch-off. The results of this research show good correlation with the nodal analysis he presented up to the point of transition.

2. A refinement to the transition between Rayleigh and Weber breakup (or varicose and sinuous) has been suggested based on the pinch-off geometry rather than the shortening of the column breakup length.

3. The frequency of pinch-off events is tied closely to the exit velocity. The frequency of pinch-off occurrences was observed to increase with increasing jet exit velocity.

4. The abrupt lengthening of the jet was observed to be a competition between the two breakup modes described – the pinching droplet and the pinching jet. In the region of transition where both modes coexist, the jet was observed to break up farther upstream from where a pinching droplet was observed to separate. The swapping back and forth between these two locations is suggested to be the reason that others have reported an abrupt lengthening, which is attributed to their inability to capture the breakup of the jet with high-speed imaging.

5. The jet breakup length has heretofore been ambiguous as three different definitions are currently in use. By observing the high-speed images, the maximum intact jet length was recorded as well as the location of pinch-off. The difference in these two values gives an indication of what is happening in the pinch-off region. When the difference in l_b and l_a is large, the mode is seen to be mixed. The difference is smaller when the pinch-off mode is singular, that is either a pinching droplet or a pinching-jet.

6. The upstream and downstream cone angles are closely tied to the ratio of the jet just prior to pinch-off and the droplet or jet that is pinching off from the main jet. The majority of the pinch-off events is seen to switch from mostly pinching droplets to

mostly pinching jets when this ratio equals 1 which is also where the upstream and downstream cone angles are equal. The correlation for the diameter ration in the transition region and up to atomization is herein reported. A preference for the pinching jet over a pinching droplet is shown when the upstream cone angle exceeds the downstream cone angle.

7. Final droplet diameters after complete jet disintegration are seen to be relatively constant within the Rayleigh breakup regime. As transition is reached, the droplets become smaller and continue to shrink in size through the transition and into the sinuous breakup regime. Beyond the point of transition, the droplets observed in the present study were seen to be much smaller than the ratios presented by Das (1997). This is attributed to the pinching-jet.

8. Satellite droplets were observed for every test condition studied. Multiple satellite droplets were seen as We increased with the most satellites seen after the transition to a pinching jet.

9. The neck length between the main jet and separating droplet (or jet) has not been reported on to date. The present study shows that the neck length increases with exit velocity, which is consistent with the increase in number of satellite droplets observed for higher We.

4.3 Recommendations and Future Work

Further study should take place with both reduced and expanded fields of view to conclusively determine whether or not satellite droplets exist where they are suspected to exist based on this study. Were one to follow up on this study, the ability to use several cameras with overlapping fields of view would be of great value. Additionally, a closed system would be beneficial to reduce any contaminates that may be introduced as a result of contaminates in the air such as dust or pollen.

Better control can be exercised in the fluid flow delivery by use of a syringe pump or similar device. This was not employed in the present study due to time and cost limitations as well as uncertainty in the ability of these devices to deliver at high enough pressures.

Further study should be made to determine whether or not the neck reaches a maximum length and again shortens, like the jet breakup length, or if the neck length continues to grow with increased We. Additional expansion of this study to include smaller diameter orifices would also be of great benefit. Research on nano-jets has begun using computational methods, but no experimental data has been found to validate those results to date.

Additionally, the present setup was used to encourage future work in internal flow visualization using PIV. The indices of refraction of both the jetting fluid and ambient

were matched in order to provide a clear, unobstructed view through the liquid jet. This is quite conducive to study the internal flow field using PIV techniques.

References

Anwar, M. M., Bright, A., Das, T. K. and Wilkinson, W. L., 1982, "Laminar Liquid Jets in Immiscible Liquid Systems." Transactions of the Institution of Chemical Engineers No. 60, pp. 306-313.

Asai, S., Hatanaka, J., Maeda, H. and Tani, T., 1988, "Mass Transfer in a Liquid-Liquid Jet with Cocurrent Laminar Flow." Chemical Engineering Science Vol. 43, pp. 713-718.

Baroud, C. N. and Willaime, H., 2004, "Multiphase Flows in Microfluidics." C. R. Physique 5 pp. 547-555.

Chesnokov, Y. G., 2000, "Nonlinear Development of Capillary Waves in a Viscous Liquid Jet." Technical Physics Vol. 45 No. 8, pp. 987-994.

Christiansen, R. M., 1955, *The Influence of Interfacial Tension on the Breakup of a Liquid into Liquid Jet*. Ph.D. thesis, University of Pennsylvania, Philadelphia Pennsylvania.

Cohen, I., Brenner, M. P., Eggers, J. and Nagel, S. R., 1999, "Two Fluid Drop Snap-Off Problem: Experiments in Theory." Physical Review Letters Vol. 83, No. 6, pp. 1147-1150.

Coyle, R. W., Berg, J. C. and Niwa, J. C., 1980, "Liquid-Liquid Jet Breakup Under Conditions of Relative Motion, Mass Transfer and Solute Adsorption." Chemical Engineering Science, Vol. 36, pp. 19-28.

Crow, E. L., Davis, F. A. and Maxfield, M. W., 1960, *Statistics Manual*. Dover Publications, New York, pp. 230-232.

Das, T. K., 1989, "Drop Formation from Expanding Jets in Immiscible Liquid Systems." ILASS-Americas 3rd Annual Conference –Extended Abstracts, Irvine, CA pp. 109-113.

Das, T. K., 1997, "Droplet Formation with Single and Multiple Nodes from a Liquid Jet in Immiscible Liquids." Atomization and Sprays, Vol. 7 pp. 407-415.

Duda, J. L. and Vrentis, J. S. 1967, "Fluid Mechanics of Laminar Liquid Jets." Chemical Engineering Science 22, 855-869.

Eggers, J., 1997, “Nonlinear Dynamics and Breakup of Free-Surface Flows.” Reviews of Modern Physics, Vol. 69, No. 3, pp 865-929.

Ganan-Calvo, A. M and Barrero, A., 1999, “A Novel Pneumatic Technique to Generate Steady Capillary Microjets.” Journal of Aerosol Science, Vol. 30, No. 1, pp. 117-125.

Gaspodinov, P., Radev, S. and Penchev, I., 1978, “Velocity Profiles and Form of a Laminar Jet in Immiscible Liquid-Liquid Systems.” International Journal of Multiphase Flow, Vol. 5, pp. 87-99.

Heertjes, P. M., de Nie, L. H. and de Vries, H. J., 1971a, “Drop Formation in Liquid-Liquid Systems – I Prediction of Drop Volumes at Moderate Speed of Formation.” The Chemical Engineering Science, Vol. 26, Iss. 3, pp. 441- 449.

Heertjes, P. M., de Nie, L. H. and de Vries, H. J., 1971b, “Drop Formation in Liquid-Liquid Systems – II Testing of the Considerations Given in Part I, for Drop Volumes below the Jetting Velocity. A Criterion for the Jetting Velocity.” The Chemical Engineering Science, Vol. 26, Iss. 3, pp. 451- 459.

Ho, L. W., Marchetti, J. and Gallegos, C., 1999. “Stability Criterion for Microscale Concentric Flow of Two Immiscible Liquids.” 1999 Modeling and Simulation of Microsystems Conference, April 19-21, 1999. San Juan, Puerto Rico.

Homma, S., Tryggvason, G., Koga, J. and Matsumoto, S., 1998, “Formation of a Jet in Liquid-Liquid System and its Breakup into Drops.” FEDSM98-5216, Proceedings of FEDSM ’98. 1998 ASME Fluids Engineering Division Summer Meeting June 21-25, 1998, Washington, DC.

Kowalewski, T. A., 1996, “On the Separation of Droplets from a Liquid Jet.” Fluid Dynamics Research 17, pp. 121-145.

Lin, S. P., 2003, “Breakup of Liquid Sheets and Jets.” Cambridge University Press, Cambridge.

Lister, J. R. and Stone, H. A., 1998, “Capillary Breakup of a Viscous Thread Surrounded by Another Viscous Fluid.” Physics of Fluids, Vol. 10, Number 11, pp. 2758 – 2764.

Liu, H., 2000, *Science and Engineering of Droplets – Fundamentals and Applications.* William Andrew Publishing, Norwich, NY.

Longmire, E. K., Norman, T. L. and Gefroh, D. L., 2001, “Dynamics of Pinch-Off in Liquid/Liquid Jets with Surface Tension.” International Journal of Multiphase Flow 27, pp. 1735-1752.

McCarthy, M. J. and Molloy, N. A., 1974, “Review of the Stability of Liquid Jets and the Effects of Nozzle Design.” The Chemical Engineering Journal, 7 pp. 1-20.

Meister, B. J. and Scheele, G. F., 1969a, “Prediction of Jet Length in Immiscible Liquid Systems.” AIChe Journal, Vol. 15, Issue 5, pp. 689-699.

Meister, B. J. and Scheele, G. F., 1969b, “Drop Formation from Cylindrical Jets in Immiscible Liquid Systems.” AIChe Journal, Vol. 15, Issue 5, pp. 700-706.

Merrington, A. C. and Richardson, E. G., 1947, “The Breakup of Liquid Jets.” The Proceedings of the Royal Socciety, Vol. 59 Part 1, No. 331, pp. 1-13.

Milosevic, I. N. and Longmire, E.K., 2002, “Pinch-Off Modes and Satellite Formation in Liquid/Liquid Jet Systems.” International Journal of Multiphase Flow 28, pp. 1853-1869.

Pimbley, W. T. and Lee, H. C., 1977, “Satellite Droplet Formation in a Liquid Jet.” IBM J. Res. Develop., 21-30.

Rayleigh, L., 1879, “On the Capillary Phenomena of Jets.” Proceedings of the Royal Society of London, Vol. 29, pp. 71-97.

Rayleigh, L. and Strutt, J. W., 1878, “On the Instability of Jets.” Proceedings of the London Mathematical Society, Vol. 10, pp. 4-13.

Razumovski, N. A., 1993, “Shape of Drops and Satellite Droplets Formed as a Result of Forced Capillary Breakup of a Liquid Jet.” Technical Physics Vol. 38 No. 9, 752-761.

Richards, J. R., Beris, A. N. and Lenhoff, A. M., 1993, “Steady Laminar Flow of Liquid-Liquid Jets at High Reynolds Numbers.” Physics of Fluids 5 (7), pp. 1703-1717.

Richards, J. R., Beris, A. N. and Lenhoff, A. M., 1995, “Drop Formation in Liquid-Liquid Systems Before and After Jetting.” Physics of Fluids 7 (11), pp. 2617-2630.

Richards, J. R., Lenhoff, A. M and Beris, A. N., 1994, “Dynamic Breakup of Liquid-Liquid Jets.” Physics of Fluids 6 (8), pp. 2640-2655.

Teng, H. C., Kinoshita, M. and Masutani, S. M., 1995, “Prediction of Droplet Size from the Breakup of Cylindrical Liquid Jets.” International Journal of Multiphase Flow, Vol. 21, No. 1, pp. 129-136.

Tjahjadi, M., Stone, H. A. and Ottino, J. M., 1992, “Satellite and Subsatellite Formation in Capillary Breakup.” Journal of Fluid Mechanics, Vol 243, pp. 297-317.

Tyler, E., 1933, “Instability if Liquid Jets.” The London, Edinburgh and Dublin Philosophical Magazine and Journal of Science, Vol. 16, Iss. 105, pp. 504 – 519.

Tyler, E. and Richardson, E. G., 1925, “The Characteristic Curves of Liquid Jets.” Proceedings of the Physical Society of London, Vol. 37 pp. 297-311.

Tyler, E. and Watkin, F., 1932, "Experiments with Capillary Jets." The London, Edinburgh and Dublin Philosophical Magazine and Journal of Science, Vol. 14, Iss. 94, pp. 849 – 881.

Vago, N., Spiegel, A., Couty, P., Wagner, F. R. and Richerzhagen, B., 2003, "New Technique for High-Speed Microjet Breakup Analysis." Experiments in Fluids 35, pp. 303-309.

Vahedi Tafreshi, H. and Pourdeyhimi, B., 2003, "The Effects of Nozzle Geometry on Waterjet Breakup at High Reynolds Numbers." Experiments in Fluids 35, pp. 364-371.

Webster, D. R. and Longmire, E. K. 2001, "Jet Pinch-Off and Drop Formation in Immiscible Liquid-Liquid Systems." Experiments in Fluids 30, pp. 47-56.

Yu, H. and Scheele, G.F., 1975, "Laminar Jet Contraction and Velocity Distribution in Immiscible Liquid-Liquid Systems." International Journal of Multiphase Flow Vol. 2, pp. 153 – 169.

Zhang, D. F. and Stone, H. A., 1997, "Drop Formation in Viscous Flows at a Vertical Capillary Tube." Physics of Fluids 9 (8), pp. 2234-2242.

Zhang, W. W. and Lister, J. R., 1999, "Similarity Solutions for Capillary Pinch-Off in Fluids of Differing Viscosity." Physical Review Letters, Vol. 83, Number 6, pp. 1151-1154.

Zhang, X. and Basaran, O. A., 1995, "An Experimental Study of Dynamics of Drop Formation." Physics of Fluids 7 (6), June 1995, pp. 1184-1203.

Appendix A

Table A-1 Pinch-Off Event Frequency Data

We	We/We*	We*	t	*f* (Hz)
6	499.049	0.136	0.056	17.937
134	432.026	0.310	0.034	29.034
146	537.036	0.272	0.107	9.380
188	940.152	0.200	0.050	20.154
233	1182.828	0.197	0.080	12.521
254	744.910	0.341	0.034	29.629
518	1516.985	0.341	0.089	11.286
553	1161.778	0.476	0.020	49.684
603	505.967	1.192	0.004	254.542
705	603.021	1.169	0.015	66.557
961	453.048	2.121	0.015	68.119
1013	698.417	1.450	0.019	53.139

Table A-2 Breakup Length Data

PSI	U (m/s)	Re	We	l_a	l_a / d_j	d_d	d_d / d_j	dmaj/dmin	l_b	l_b / d_j	l_b-l_a	MODE
0	1.73	26.8563	11	2.41262	24.7652	3.14197	32.2518	1.11897	5.42246	55.6607	3.00984	1
2	6.57	99.4828	164	9.01004	92.4865	1.94209	19.9352	1.19596	10.754	110.388	1.74399	1
12	10.94	165.637	456	13.67	140.321	1.88971	19.3976	1.16376	16.8077	172.528	3.13768	2
16	11.17	169.177	475	11.6376	119.458	1.44772	14.8606	1.0703	14.765	151.56	3.12739	2
20	13.41	203.179	685	16.2536	166.841	1.58197	16.2386	1.23512	20.1886	207.233	3.935	2
38	16.64	252.105	1055	16.6911	171.331	1.23953	12.7235	1.18911	20.889	214.422	4.19795	3
45	19.18	290.565	1402	13.7193	140.826	0.82681	8.48705	1.1057	16.7091	171.516	2.98984	3
56	19.621	297.196	1467	11.0058	112.972	0.71174	7.30585	1.15021	13.3019	136.542	2.29614	3
72	22.053	334.037	1853	7.63148	78.3358	0.60671	6.22774	1.25999	10.5082	107.865	2.87675	4

Table A-3 Conditions at Pinch-Off

Re	We	We^*	d_d^* (mm)	d_j^*	V_d^* (mm^3)	d_d^*/d_j^*	θ_u	θ_d
64	68	0.136	1.860	0.774	3.371	2.407	77.801	137.120
90	134	0.310	1.462	0.737	1.636	1.956	87.741	134.684
94	146	0.272	2.244	0.791	5.920	2.792	88.638	131.291
106	188	0.200	1.877	0.955	3.460	1.983	74.966	131.218
118	233	0.197	2.020	1.030	4.318	2.003	73.246	132.709
124	254	0.341	2.010	0.883	4.252	2.276	65.842	129.822
177	518	0.341	1.933	1.110	3.648	2.671	100.140	126.440
182	553	0.476	1.679	1.006	2.993	1.667	70.308	121.528
186	596	0.612	1.472	0.947	1.670	1.549	78.178	111.694
190	603	1.192	0.858	0.776	0.386	1.109	93.533	107.274
206	705	1.169	0.854	0.823	0.326	1.052	92.344	103.254
241	961	2.121	0.503	0.748	0.067	0.805	102.912	70.176
247	1013	1.450	0.337	0.867	0.020	0.389	112.036	51.404

Table A-4 Parent Droplet Data

Re	We	We^*	d_d	d_d/d_j	d_d/d_j^*	d_j^*/d_j^*	d_d/d_d^*
64	68	0.136	1.816	18.639	2.347	1.000	0.976
90	134	0.310	1.462	15.006	1.983	1.000	1.000
94	146	0.272	2.368	24.309	2.992	1.000	1.055
106	188	0.200	1.840	18.885	1.927	1.000	0.980
118	233	0.197	1.945	19.961	1.887	1.000	0.963
124	254	0.341	1.931	19.818	2.186	1.000	0.961
177	518	0.341	1.923	19.735	1.732	1.000	0.995
182	553	0.476	1.481	15.197	1.472	1.000	0.882
186	596	0.612	2.240	22.996	2.364	1.000	1.522
190	603	1.192	0.802	8.230	1.033	1.000	0.934
206	705	1.169	0.831	8.531	1.010	1.000	0.974
241	961	2.121	1.500	15.397	2.004	1.000	2.983
247	1013	1.450	1.517	15.574	1.750	1.000	4.497

Table A-5 Das (1997) Data and Present study at log (μ_d/μ_a) = -0.818, $y = d_d/d_j^*$

N=3		N=2		N=1		Present Study*	
x	y	x	y	x	y	x	y
-3.04	3.80	-3.02	3.31	-3.02	2.64	-0.818	1.816
-2.05	3.24	-2.02	2.84	-2.02	2.25	-0.818	1.462
-1.03	2.90	-1.03	2.54	-1.03	2.02	-0.818	2.368
-0.31	2.88	-0.31	2.52	-0.31	2.00	-0.818	1.840
-0.06	2.91	-0.06	2.55	-0.06	2.02	-0.818	1.945
-0.03	2.92	-0.03	2.55	-0.01	2.02	-0.818	1.931
0.68	3.08	0.68	2.69	0.68	2.13	-0.818	1.923
0.98	3.25	0.98	2.85	0.98	2.25	-0.818	1.481
1.28	3.42	1.28	2.99	1.28	2.38	-0.818	2.240
2.00	3.87	2.00	3.38	2.02	2.69	-0.818	0.802

*Present data only shown up to region where breakup is mostly jet pinch-off

Table A-6 Satellite Frequency and Diameter Data

u* (mm/s)	V dot mm3/s)	Re	We	We*	d sat 1	d sat 2	d sat 3	% Occurrences one satellite	% Occurrences two satellites	% Occurrences three satellites	% Occurrences no satellites
67.079	31.540	64	68	0.136	0.044			100	0	0.000	0.000
103.679	44.260	90	134	0.310	0.037			84.61538462	0	0.000	15.38461538
93.683	46.090	94	146	0.272	0.032			100	0	0.000	0.000
73.150	52.380	106	188	0.200	0.055			57.14285714	42.85714286	0.000	0
69.890	58.280	118	233	0.197	0.055	0.036		72.7273	27.2727	0.000	0.000
99.324	60.840	124	254	0.341	0.064			100	0	0.000	0
88.648	85.820	177	518	0.341	0.064	0.045		88.23529412	11.76470588	0.000	0.000
109.975	87.340	182	553	0.476	0.077	0.116		73.913	4.3478	0.000	21.7391
128.444	90.560	186	596	0.612	0.105	0.080		47.8261	4.3478	0.000	47.8261
198.041	93.760	190	603	1.192	0.065	0.060		92.8571	7.1429	0.000	0.000
190.502	101.370	206	705	1.169	0.088			100	0	0.000	0
269.099	118.390	241	961	2.121	0.061	0.027	0.140	46.2962963	24.07407407	1.851851852	27.77777778
206.763	122.030	247	1013	1.450	0.043			100	0	0.000	0.000

Table A-7 Neck Length Data

Re	We	We^*	l_n (mm)	l_n/d_j^*
64	68	0.136	0.200	0.259
90	134	0.310	0.120	0.163
94	146	0.272	0.113	0.142
106	188	0.200	0.222	0.232
118	233	0.197	0.235	0.228
124	254	0.341	0.193	0.219
177	518	0.341	0.258	0.232
182	553	0.476	0.289	0.287
186	596	0.612	0.327	0.346
190	603	1.192	0.328	0.423
206	705	1.169	0.363	0.441
241	961	2.121	0.271	0.362
247	1013	1.450	0.218	0.251

Table A-8 Percentage of Occurrences of Pinch-Off Type

Re	We	We*	Drop	Jet
64	68	0.136	100.000	0.000
90	134	0.310	100.000	0.000
94	146	0.272	100.000	0.000
106	188	0.200	100.000	0.000
118	233	0.197	100.000	0.000
124	254	0.341	100.000	0.000
177	518	0.341	82.353	11.765
182	553	0.476	87.879	12.121
186	596	0.612	88.889	11.111
190	603	1.192	85.714	14.286
206	705	1.169	78.571	21.429
241	961	2.121	16.670	83.330
247	1013	1.450	0.000	100.000

Table A-9 Description of Modes of Pinch-Off Observed

Mode	Description
1	Pinching Droplet
2	Bi-Modal
3	Pinching Jet
4	Atomization